Histone lactylation: a new epigenetic mark in the malaria parasite *Plasmodium*

Ibtissam Jabre[1a] & Nana Efua Andoh[1a], Juliana Naldoni[1], William Gregory[1], Chae Eun Yoon[2,3], Aubrey J. Cunnington[2,3], Athina Georgiadou[2,3], Andrew M. Blagborough[1], Catherine J. Merrick[1*]

[1] Department of Pathology, University of Cambridge, Tennis Court Road, Cambridge, CB2 1QP, UK.

[2] Section of Paediatric Infectious Disease, Department of Infectious Disease, Imperial College London, London, United Kingdom.

[3] Centre for Paediatrics and Child Health, Imperial College London, London, United Kingdom.

[a] Equal contributions

* To whom correspondence should be addressed:
Department of Pathology, Cambridge University, Tennis Court Road, Cambridge, CB2 1QP, UK
Tel: (+44) 1223 333330
CJM: Email: cjm48@cam.ac.uk

ABSTRACT

In the malaria parasite *Plasmodium falciparum,* epigenetic modifications such as acetylation and methylation play important roles in parasite biology and virulence. Here, we characterised a new epigenetic mark, histone lactylation, recently discovered in humans and also present in *Plasmodium*. It was found in two human malaria parasites, *P. falciparum* and the zoonotic macaque parasite *P. knowlesi*, and was also found *in vivo* in two rodent malaria models. Histones were lactylated rapidly in response to elevated lactate levels, either exogenously added or endogenously generated by the parasite's own metabolism, and they were rapidly delactylated when lactate levels fell. Thus, this epigenetic mark is well-placed to act as a metabolic sensor, since severe falciparum malaria characteristically leads to hyperlactataemia in infected patients. Mass spectrometry showed that lysines on several parasite histones could be lactylated, and that this was accompanied by lactylation of many non-histone chromatin proteins. Histone lactylation was less abundant and less inducible in *P. knowlesi* than in *P. falciparum*, suggesting that *P. falciparum* may have evolved particular epigenetic responses to this characteristic feature of its pathology. Finally, in the rodent model *P. yoelii*, hyperlactataemia correlated with parasite transcriptomic programmes that suggested metabolic 'dormancy'.

KEYWORDS: Malaria, *Plasmodium*, epigenetics, histone lactylation, lactyl lysine

INTRODUCTION

Human malaria has many characteristic pathological features, one of which is hyperlactataemia. This is clinically defined as a level of blood lactate above 5mM, but malaria patients can reach at least 15mM (Krishna, Waller et al. 1994, Merrick, Huttenhower et al. 2012). Parasites in the bloodstream respire by glycolysis, producing lactate, and they also cause their host erythrocytes to adhere to capillary walls, impeding blood flow and promoting anaerobic respiration in host tissues. Collectively, this results in hyperlactataemia, which is predictive of severe disease and death, as it can lead to the fatal malaria syndrome of metabolic acidosis and respiratory distress (Possemiers, Vandermosten et al. 2021).

Plasmodium parasites could benefit from being able to sense the metabolic environment in their host and modify virulence accordingly – for example, by increasing commitment to sexual stages that are competent for transmission to new hosts, or by modulating cytoadherence of infected erythrocytes. This fascinating area of host-parasite biology is increasingly being explored, with aspects of blood chemistry including levels of glucose, magnesium and S-adenosylmethionine being proposed to influence parasite virulence (Mancio-Silva, Slavic et al. 2017, Andrade, Fleckenstein et al. 2020, Harris, Tong et al. 2023, Diffendall, Claës et al. 2024).

Blood lactate has yet to be fully explored in this context, but since it correlates with parasite load and disease severity, it could potentially serve as both a 'quorum sensor' and a measure of host stress. In one human infection study, it was linked to the expression pattern of a key virulence gene family, *var*, which encodes variant adhesins expressed on infected erythrocytes (Merrick, Huttenhower et al. 2012). This gene family is known to be epigenetically controlled by histone acetylation and methylation. Epigenetics also plays other prominent roles in *Plasmodium* biology, controlling aspects of virulence including alternate invasion pathways and sexual stage commitment (gametocytogenesis) (Duraisingh and Horn 2016). In a recent *in vitro* study, gametocytogenesis was also linked to lactate, with parasites cultured in added lactate converting to gametocytes at an elevated rate (West and Sullivan 2020).

Here, we explored lactate as a potential epigenetic modifier in *Plasmodium*, following the recent discovery of lactyl-lysine as a new epigenetic mark in mammalian cells, similar to the well-characterised acetyl-lysine (Zhang, Tang et al. 2019). Since its discovery in 2019, this epigenetic mark has been heavily explored in the context of human cells in high-lactate environments – primarily tumours experiencing the Warburg effect (Su, Zheng et al. 2023, Dai, Wang et al. 2024). It has not, however, been explored in the context of malaria, a disease characterised by systemic hyperlactataemia. However, we did recently observe that histone lactylation could occur in *P. falciparum*, and hence proposed this as a new virulence modifier in *Plasmodium* (Merrick 2023). We now report that the epigenetic mark is conserved in several *Plasmodium* species, occurring both *in vitro* and *in vivo*. It appears on many histone lysine residues, is rapidly labile and is responsive to lactate levels

both in culture and in mammalian host blood. Therefore, it could have many virulence-modulating roles.

RESULTS

Plasmodium histones are inducibly lactylated

We first measured the level of lactyl-lysine in *Plasmodium* histones after treating cultured parasites with increasing levels of lactate. Trophozoite-stage *P. falciparum* parasites were exposed to 5-25mM lactate, added to the culture media for 12h, and **Figure 1A & S1A** show that their histones were inducibly and titratably lactylated. Histone H4 showed the strongest lactyl-lysine signal. An antibody identifying a single lactylated residue on histone H4 – K12 – revealed a similar pattern, although lactylation of this residue was much less strongly inducible than the histones as a whole **(Fig 1B, S1B)**. We conducted the same experiments on a second species, *P. knowlesi*, and showed that histone lactylation was similarly inducible **(Fig 1C, S1C)**, but much less abundant than in *P. falciparum*, since greater amounts of parasite extract were required to detect similar signals on *P. knowlesi* histones, and the specific residue H4K12La was barely detectable **(Fig S1C,D)**.

We then investigated whether this phenomenon occurs naturally *in vivo* during malaria. The rodent model species *P. yoelii*, strain 17XL, can generate severe hyperlactataemia (Georgiadou, Dunican et al. 2022), and blood lactate levels in mice infected with *P. yoelii* 17XL did indeed correlate with histone lactylation in the parasite **(Fig 1D)**. Notably, not all rodent malaria models lead consistently to hyperlactataemia and in the *P. berghei* ANKA strain, which does not (Georgiadou, Dunican et al. 2022), we did not observe a strong correlation between blood lactate and histone lactylation **(Fig S1E)**. Overall, these results revealed that there is a conserved pathway for histone lactylation in *Plasmodium,* induced by conditions of hyperlactataemia.

Histone lactylation is rapidly inducible and reversible

We next investigated the time dynamics of the modification: **figure 1** shows that it can occur within 12h and 8h in *P. falciparum* and *P. knowlesi* respectively*,* but it does not show how fast the modification was actually added, or how fast it would be removed if exogenous lactate levels subsequently fell. To investigate this, parasites were tightly synchronised at rings, washed into fresh media, exposed to a pulse of 25mM lactate when they reached early trophozoites, and then followed by western blotting at intervals over the subsequent 36h. (25mM lactate was chosen for these and subsequent experiments because, from **figure 1**, this induced the strongest histone lactylation, without inhibiting parasite growth, whereas even higher levels (≥ 30mM) could affect parasite growth ((Hikosaka, Hirai et al. 2015) and data not shown)). **Figures 2A & S2A** show that histone lactylation rose within just 2h of exposure; continued to rise after 6h, and then fell back slightly after 12h. This was surprising, but we surmised that it may be because of a natural cell-cycle-related pattern in histone lactylation, since parasite metabolism produces its own endogenous lactate. This

was confirmed by an identical parallel timecourse in which no exogenous lactate was added **(fig 2A, S2A**: grey bars**)**: histone lactylation was still induced, to a much lesser extent, peaking in the mid-trophozoite stage (~30-32hpi) and falling back slightly in late trophozoites (~36-38hpi). The specific residue H4K12 showed similar dynamics of lactylation in response to 25mM lactate **(fig 2B)**, but its induction was not as strong as induction of KLa overall **(fig S2B)** and lactylation of this residue was not induced at all during a non-lactate-treated cell cycle **(fig 2B, S2B)**.

To measure the dynamics of de-lactylation, parasite cultures were washed after 12h and then followed at three subsequent timepoints 6, 12 and 24h later (re-washing at each of these points to keep the lactate levels in the media low). By 6h (i.e. in schizonts at ~42-44hpi), the level of histone lactylation had reverted to baseline levels. Again, this followed the 'natural' cell cycle pattern, which was greatly amplified by exposure to exogenous lactate. Thus, histone lactylation was rapidly responsive – in both directions – to changes in the lactate content of the media.

We repeated these experiments in *P. knowlesi,* with similar results **(fig 2C,D; S2C)**: histone lactylation was inducible across the trophozoite stage of the cell cycle, but the background levels of lactylated histones in parasites unexposed to exogenous lactate were low, variable, and not clearly cell-cycle-regulated in this species **(fig 2C, S2C)**. Furthermore, in this species, H4K12 showed no consistent pattern or induction of lactylation **(fig 2D)**. As in **figure 1**, when compared to *P. falciparum*, 4-5 times the quantity of *P. knowlesi* histones was required to detect comparable levels of histone lactylation by western blotting.

To measure the extent of endogenous lactate production in our parasite culture system, we measured lactate levels in the media, both when parasites were cultured under standard conditions (reducing the parasitaemia and changing the media every 48h), and also when they were allowed to grow continuously to the point of 'crashing' **(fig 2E,F)**. As expected, media lactate levels correlated with parasitaemia, reaching ~5mM within 2 days as a culture of *P. falciparum* grew from 0.5% to 4.6% parasitaemia **(fig 2E)**. When the culture was allowed to 'crash', lactate levels peaked at ~10mM **(fig 2E)**. We also followed histone lactylation over 72h by western blotting, confirming that it fluctuated in a stage-dependent manner even as lactate accumulated in the media, with lactylation consistently higher in trophozoites and lower in rings **(fig 2G, S2D).** The profile of lactate production was similar in *P. knowlesi* cultures, although this parasite is more resistant than *P. falciparum* to 'crashing' (i.e. parasite death caused by exposure to spent media), so these parasites could grow exponentially for at least 3 days, producing lactate continuously and reaching 11.5mM by day-4 **(fig 2F)**.

Overall, these data show that routine culture of both parasite species can expose them to significant but modest lactate fluctuations. Routine cultures can reach the clinical threshold for hyperlactataemia (5mM), which is sufficient to induce some histone lactylation **(fig 1)**, but is much lower than the levels attained in human patients with severe malaria (Krishna, Waller et al. 1994, Merrick, Huttenhower et al. 2012).

Histone acetylation is affected by exposure to high lactate

In human cells, both acetylation and lactylation have been detected on the same histone lysine residues, and it has been suggested that histone acetyltransferase enzymes may moonlight as lactylases (Zhang, Tang et al. 2019). This raised the possibility that in *Plasmodium*, histone lactylation could reciprocally affect histone acetylation – a well-established factor in gene expression regulation.

We tested this by western-blotting for acetyl H4 and acetyl H3 under conditions of high lactate exposure, as in **figure 1. Figure 3A,B** shows that histone H3 in *P. falciparum* was inducibly acetylated, rising ~2-fold after exposure to 10-25mM lactate, while H4 acetylation was induced ~3-fold, starting at 5mM and peaking at 10-25mM lactate. These changes were lower than the changes in histone lactylation measured in the same parasites (~5-fold, **fig 1**), and they were also somewhat weaker in a replicate experiment **(Fig S3A,B)**, but neverthless the two histone marks were apparently mutually regulated by lactate. By contrast, in *P. knowlesi*, histone acetylation changed little after exposure to exogenous lactate **(fig 3C,D; S3C,D)**.

We also followed the time dynamics of histone acetylation following lactate exposure, using timecourses as in **figure 2** (**fig 3E-H)).** In *P. falciparum*, acetylation did not vary greatly across the normal cell cycle (fluctuations were less than 2-fold for both H3Ac and H4Ac, although H3Ac did rise slightly in trophozoites, similar to lactylation). After exposure to 25mM lactate, histones were additionally acetylated. This occured as rapidly as lactylation – within 2h – but deacetylation was not equally rapid after lactate removal **(fig 3E,F; S3E,F)**. This may suggest that histone acetyltransferase activity is shared for both modifications, whereas deacetylase activity is not. In *P. knowlesi,* as expected from the results in **figure 3C and D**, exogenous lactate had little influence on histone acetylation across the cell cycle **(fig 3G,H; S3G,H)**.

Histone lactylation is distributed throughout the nucleus

In *P. falciparum,* certain histone modications are specifically associated with heterochromatin, which tends to be located at the nuclear periphery, marked by heterochromatin protein 1 (HPI) (Flueck, Bartfai et al. 2009), whereas other modifications associated with euchromatin appear throughout the nucleoplasm. We investigated the location of histone lactylation using immunofluorescence microscopy **(fig 4)**. We found no evidence for compartmentalisation of lactylated histones, with both the general lactyl-lysine signal **(fig 4A)** and the specific signal for H4K12 **(fig 4B)** appearing throughout the nuclei of all parasite stages. Neither signal colocalised with HP1, and both appeared similar to the pan-nuclear distribution of histone acetylation (**fig S4**). The great majority of lactyl-lysine signal was nuclear **(fig 4A)**, suggesting that there is little lactylated protein in the cytoplasm of *Plasmodium.*

Histone lactylation occurs on multiple histone lysine residues

For a comprehensive view of the histone lysine residues that can be lactylated in both *P. falciparum* and *P. knowlesi*, we used liquid chromatography-tandem mass spectrometry (LC-MS/MS). Trophozoite-stage parasites were either exposed or not exposed to 25mM lactate and their histones were acid-extracted from chromatin in biological triplicate. In a single pilot experiment, histones were also extracted from mixed stage cultures (+/- 25mM lactate), enabling detection of KLa sites in all stages of the asexual cycle. Histone integrity and the induction of lactylation were confirmed via Coomassie-stained SDS-PAGE and by immunoblotting for KLa **(Fig S5)**.

Mass spectrometry on the histone-containing region of the gel identified all eight histones (H2A, H2A.Z, H2B, H2B.Z, H3, H3.3, CenH3 and H4), with sequence coverage >67.5% except in the case of CenH3 **(Tables S1-4).** We then mapped KLa sites, as previously reported (Zhang, Tang et al. 2019) **(Fig S6A)**, revealing 16 and 21 KLa sites in *P. falciparum* and *P. knowlesi* respectively **(Fig 5A)**. These were unevenly distributed across the histone tails and almost all KLa sites could also be acetylated **(Fig S6B, Tables S1-4).** Interestingly, despite the histone sequences being highly conserved between *Plasmodium* species, the majority of KLa sites were species-specific, suggesting that this modification may have species-specific function(s). As expected from **figures 1-2**, lactylation of some residues was induced after exposure to 25mM lactate, but inducibility varied between residues and also between species **(fig 5B).** It also varied in trophozoites versus mixed-stage cultures, implying that some residues may be lactylated stage-specifically.

<u>Cross-talk may occur between histone lactylation, acetylation and methylation</u>

Acetylation and lactylation were often detected on the same lysine residues, both in our data and previously in human cells (Zhang, Tang et al. 2019). Therefore we sought to investigate whether lactate exposure in the trophozoite stage could induce changes in the distribution of histone acetylation (Kac), as well as di- and tri- methylation (K(me2), K(me3)).

There was no dramatic change in the distribution of Kac sites after exposure to 25mM lactate, and Kac remained the most abundant histone modification, as previously reported (Trelle, Salcedo-Amaya et al. 2009) **(Tables S1-4)**. Almost all KLa sites were also detected as Kac but the converse was not true: ~65% of Kac sites were unique **(Fig S6B)**. After lactate exposure, 44% of histone KLa sites in *P. falciparum* and 17% of those in *P. knowlesi* were significantly induced (P-value ≤ 0.05) **(fig 6A, top panel; Tables S1-2)**, corroborating the observation from **figures 1-2** that lactylation was more strongly inducible in *P. falciparum* than in *P. knowlesi.* By contrast, only ~12% and ~7% of histone Kac sites, respectively, were significantly up- or down-regulated. Hence, relatively few Kac sites (amongst many that can be acetylated) must be responsible for the rise in total histone acetylation after lactate exposure that was detected by western blot in **figure 3**. Overall, KLa was clearly the most inducible post-translational mofification (PTM) after lactate exposure (**fig S7A)**, and sites that were strongly induced as lactylated were not simultaneously induced as acetylated **(fig S7B)**.

In contrast to Kac, major changes did occur in K(me2) and K(me3): ~90% of these sites were significantly down-regulated in *P. falciparum* after lactate exposure **(fig 6A, lower panel; Tables S1-2)**. This was not the case in *P. knowlesi,* where no reciprocal changes in K(me2) and K(me3) were seen.

Non-histone chromatin-associated proteins can be lactylated

Chromatin-associated proteins besides histones appeared in the mass spectrometry data, and many of these were also lactylated, with a subset of the modifications being induced after exogenous lactate exposure **(Fig 6B, Tables S3-4)**. In *P. falciparum*, lactylated sites were found in chromatin-bound proteins such as Alba3, several RNA helicases, proteins implicated in epigenetics (e.g. histone deacetylase 2), in glycolytic metabolism (e.g. glycerol-3-phosphate dehydrogenase) and in transcriptional control (e.g. two ApiAP2 transcription factors). A third AP2 factor, ApiAP2G, which induces gametocytogenesis, was also detected as lactylated, but its coverage fell below the threshold for inclusion (data not shown), probably due to its very low expression in these asexual-stage cultures. An acetyl-CoA transporter was also lactylated, suggesting again the possibility of cross-talk between acetyl and lactyl epigenetic pathways **(Fig S8A; Table S3)**. In *P. knowlesi*, most of the same proteins were not detected as lactylated, although other proteins, including the acetyltransferase GCN5, were **(Fig S8B; Table S4).**

Although almost all the lactylated lysines within histones could also be acetylated **(fig S6B)**, this was not the case in non-histone proteins. Unique, lactate-induced KLa sites appeared on several chromatin-associated proteins. These included epigenetic regulators (e.g. SAP18, associated with HDAC1) and RNA binding proteins such as Alba4 in the case of *P. knowlesi*, and RNA helicases (e.g. NAM7, responsible for RNA turnover), RNA binding proteins, AP2 transcription factors and gametocytogenesis factors (e.g. Male Development 1) in the case of *P. falciparum* **(Table S1-2)**.

Collectively, it appeared that the KLa modification was widespread, both on histones and on other proteins. It was modulated on some proteins by exogenous lactate, but also probably derived from lactate produced by the parasite. The wide range of lactylated proteins suggests that the modification could regulate multiple aspects of *Plasmodium* biology, from epigenetics to RNA biology to protein function.

Lactyl post-translational modification does not correlate with levels of protein expression

There was no consistent correlation between proteins that were inducibly modified and proteins that changed in abundance after exposure to 25mM lactate (**fig S9**). In *P. knowlesi*, no histones and very few other proteins showed significant changes (with a sca.*P*-value ≤ 0.01) after lactate exposure; in *P. falciparum*, a few proteins did change significantly in abundance, including histone H2A.Z and HP1, and interestingly the changes were mostly downregulation (**fig S9A**). Overall, however, there was no correlation between proteins whose PTMs were significantly changed, and proteins that changed in abundance (**fig S9B**).

Proteins in different biological pathways are lactylated in *P. falciparum* versus *P. knowlesi*

It was apparent that the epigenetic marks affected by lactate exposure, both on histones and on non-histone proteins, differed in *P. falciparum* versus *P. knowlesi.* Gene ontology (GO) enrichment analysis was therefore performed to gain insight into the pathways most affected in each species.

Amongst the proteins whose epigenetic marks changed after lactate exposure, many different biological functions were found to be enriched *(P*-value ≤ 0.05), depending on both the species and the epigenetic modification (KLa, Kac or Kme). In *P. falciparum,* lactate-modulated KLa sites were significantly enriched in proteins involved with metabolism of tRNAs and indole compounds, for example; in *P. knowlesi,* the top GO terms associated with such KLa sites included 'cell growth', 'cell division' and 'autophagy' **(fig 7A, fig S10, Table S5)**.

Amongst GO terms for cellular components, KLa sites, as well as Kac and Kme sites, that responded to lactate exposure were enriched in proteins involved with the nucleosome and protein-DNA complexes. This was not surprising given the known predominance of such PTMs on histones, as well as the location of KLa observed in **figure 4** – almost exclusively nuclear. In *P. knowlesi*, there was also an interesting enrichment of lactate-modulated KLa sites in the carbon CCR4/Not complex, which regulates aspects of protein function, RNA metabolism and transcriptional activity during late gametocyte differentiation and post-fertilization development (Hart, Power et al. 2021) **(fig 7B, fig S11, Table S5).** Amongst molecular function GO terms, both species showed enrichment of 'protein dimerization' and 'catalytic activity', amongst others **(fig S12, Table S5)**.

Blood lactate levels in malaria-infected mice correlate with distinct transcriptomic profiles in the causative parasites

In **figure 1D**, we investigated a rodent malaria model that becomes severely hyperlactaemic, *P. yoelii* 17XL, and showed that histone lactylation in the parasites was strongly induced in hyperlactaemic hosts. Using this model, RNAseq analysis had previously been conducted in groups of mice with early-stage versus late-stage infections (i.e. low versus high blood lactate) (Georgiadou, Dunican et al. 2022). We re-analysed those data for the parasite (rather than the host) transcriptome, seeking changes that correlated with high histone lactylation in late-stage infections. For comparison, we analysed the same data from *P. berghei* ANKA, where late-stage infections did not consistently generate hyperlactataemia (Georgiadou, Dunican et al. 2022). All datasets were first corrected for different mixes of parasite developmental stages (Tebben, Dia et al. 2022), and indeed marked differences in the proportions of schizonts were detected in early versus late-stage *P. yoelii* infections, while gametocytes were found in low proportions in early infections but were undetectable in late infections **(Table S6).**

Differential expression (DE) analysis (Calixto, Guo et al. 2018) performed on the corrected data revealed distinct expression profiles in late versus early stages of infection in

both species **(fig S13A)**. Large cohorts of genes were differentially expressed (*P*-value ≤0.05): 502 genes in *P. yoelii* (238 upregulated and 264 downregulated) and 1521 genes in *P. berghei* (803 upregulated and 718 downregulated) (**fig 8A, Table S6**). (Using more stringent criteria, *P*-value ≤0.05 and |log2FC| ≥ 1, expression changes were similarly distributed across fewer total genes **(fig S13B)**). Late-stage *P. yoelii* parasites showed a strong downregulation of the lactate dehydrogenase gene, as well as the glycolytic enzyme phosphofructokinase and several genes putatively involved in gametocytogenesis. Several tRNA synthetases were also downregulated, with the interesting exception of isoleucine tRNA synthetase (isoleucine is the only amino acid that the parasite must scavenge from its host). Indeed, genes with the strongest expression changes were generally downregulated, while fewer – including several histones – were upregulated **(fig 8B,C)**. The opposite was true in late-stage *P. berghei*, where gene upregulation was most apparent, including the upregulation of phosphofructokinase and glyceraldehyde 3-phosphate dehydrogenase, and factors involved in DNA replication and repair such as MCMs and RecQ helicase **(fig 8B,C)**.

When GO enrichment analysis was conducted on the up- and down-regulated genes, it was clear that late-stage *P. yoelii* parasites activated biological **(fig 8D)** and molecular **(fig S14)** functions including proteolysis and mono-carboxylic acid metabolism, while late-stage *P. berghei* parasites activated contrasting functions including DNA replication and repair, chromosome segregation, cell division and actin/cytoskeleton dynamics. Amongst functional pathways, late-stage *P. yoelii* parasites upregulated fatty acid metabolism whereas *P. berghei* upregulated sugar metabolism and glycolysis **(fig S14).** Thus, it appeared that *P. yoelii* parasites in hyperlactaemic hosts showed features of 'dormancy', which can be induced in *P. falciparum* by isoleucine starvation and is characterised by slowing of the replicative cycle and proteolysis (Babbitt, Altenhofen et al. 2012); whereas *P. berghei* – in hosts without hyperlactataemia – upregulated pathways involved in replication.

DISCUSSION

This work represents the first characterisation of a new epigenetic mark, histone lactylation, in the malaria parasite *Plasmodium.* A lactylation epigenetic pathway could be highly influential in the biology and pathology of malaria, because some *Plasmodium* species, including *P. falciparum*, characteristically cause hyperlactataemia in their hosts (Possemiers, Vandermosten et al. 2021). It would therefore make sense if these parasites had evolved to sense and respond to hyperlactataemia, potentially modulating their virulence or transmission dynamics.

Here, we show that histone lysine lactylation in several *Plasmodium* species is rapidly inducible by exogenous lactate, and also rapidly reversible. (These dynamics differ from those reported in mammalian macrophages, where histone lactylation was originally discovered, and where the modification occurred relatively slowly (Zhang, Tang et al. 2019).) We detected histone lactylation across four *Plasmodium* species, both *in vitro* and *in vivo*, but it was not equally prominent, nor equally responsive to exogenous lactate, in all species. Rather, it was more abundant and more inducible in species that cause hyperlactataemia: *P.*

falciparum and *P. yoelii*. In cultured *P. knowlesi*, a species that is only rarely associated with lactic acidosis in humans (Barber, Grigg et al. 2017), the modification was less abundant and was not clearly regulated across a normal cell cycle, as it was in *P. falciparum.* In *P. berghei* ANKA, which did not cause consistently high levels of hyperlactataemia in mice, the modification was not clearly responsive to blood lactate, whereas in *P. yoelii* 17XL, it was. Commensurate with profound species-specific differences, mass spectrometry showed that the histone lysine residues lactylated in *P. falciparum* and *P. knowlesi* were generally different.

In human cells, it has been suggested that lactylation may act like acetylation on histone tails – as a transcription-activating mark (Zhang, Tang et al. 2019). In *Plasmodium*, this may also be true. KLa was detected throughout nuclear chromatin, which is mainly euchromatic, with no specificity for heterochromatin. Furthermore, Kme marks are generally gene-silencing in *P. falciparum*, and mass spectrometry showed that these were mostly downregulated after lactate exposure, suggesting reciprocal regulation of KLa-induced activation and Kme-induced silencing. Again, species-specificity was apparent: such reciprocity was notably absent in *P. knowlesi.*

KLa and Kac were not, however, interchangeable: only a small subset of Kac sites in either species was detected as lactylated, and a large proportion of the KLa sites, but only a few Kac sites, were induced by exogenous lactate. This has implications for the theory that histone acetyltransferases (HATs), which normally use acetyl-CoA, can also use lactyl-CoA to act as writers of KLa (Zhang, Tang et al. 2019). Since lysine residues were not simply modified with either moiety according to substrate abundance, our results would suggest that only some HATs might use lactyl-CoA, on only some lysine sites. In fact, if conditions of high lactate do stimulate certain HATs towards lactyltransferase activity, the same conditions appear to stimulate acetyltransferase activity on a subset of residues as well, since histone acetylation rose modestly after lactate exposure. The possible contributions of *P. falciparum* HATs to lactyltransferase activity are currently being investigated. An entirely separate pathway was also recently reported, in which alanine tRNA synthetase moonlights as a lactyltransferase (Ju, Zhang et al. 2024, Zong, Xie et al. 2024) and this might also operate in *Plasmodium.*

Besides histone tail lactylation, we detected numerous non-histone proteins being lactylated. These were certainly not comprehensively surveyed because our mass spectrometry focussed on small, chromatin-associated proteins (large, nucleoplasmic or cytoplasmic proteins were probably under-detected). Nevertheless, we detected lactylation on ApiAP2 transcription factors, RNA processing factors, HATs and HDACs amongst others. Unlike the histone tails, where almost every lactylated lysine could also be acetylated, some non-histone proteins were uniquely lactylated (and again, they were largely species-specific between *P. falciparum* and *P. knowlesi*). Thus, the lactyl PTM may have evolved, species-specifically, to regulate *Plasmodium* biology on at least three levels: the epigenetic control

of gene transcription via histone tail marks, the co-transcriptional control of RNA processing, and the post-translational modulation of protein activity in HATs, HDACs, etc. – potentially biasing their enzyme activity from acetyl- to lactyl- specificity. The biological pathways that are actually regulated await investigation, because lactylated proteins were associated with a wide range of GO terms. Important pathways could potentially include stress-responsive transcriptional programmes controlled by ApiAP2s (possibly including gametocyte conversion, since lactylated ApiAP2G was detected in *P. falciparum*, albeit at a low level), and the expression of *var* genes or other virulence gene families that are epigenetically regulated via HAT/HDAC activity (Duraisingh and Horn 2016).

To gain insight into biological changes that can occur in parasites exposed to hyperlactatemia *in vivo*, we analysed transcriptomic data from *P. yoelii* in hyperlactaemic mice. Profound changes were detected, with features of metabolic dormancy – a programme previously reported in *P. falciparum* parasites starved of isoleucine, the only amino acid that malaria parasites cannot gain from haemoglobin catabolism (Babbitt, Altenhofen et al. 2012). Starved *P. falciparum* parasites slowed their developmental cycle and activated proteolysis: features also seen in the GO analysis for late-stage *P. yoelii*, but not in late-stage *P. berghei* where the hosts are not generally hyperlactaemic and the parasites do not induce high levels of histone lactylation. Future work will focus on comprehensive analyses of the transcriptome and epigenome, to establish which – if any – of the transcriptional programmes in parasites exposed to hyperlactataemia are actually epigenetically controlled by histone lactylation, or alternatively controlled by lactylation of other chromatin proteins.

DATA AVAILABILITY

Sequencing data from mouse, *P.yoelii* and *P. berghei* are available at ENA under the ID PRJEB43641 as per Georgiadou *et al*. (Georgiadou, Dunican et al. 2022).

MATERIAL & METHODS

Culture and synchronisation of *P. falciparum* and *P. knowlesi*

Plasmodium falciparum (NF54 strain) and *Plasmodium knowlesi* (A1-H.1 strain) were grown in RPMI 1640 media (Sigma, R4130) with 2.3 g/L sodium bicarbonate, 50 mg/L hypoxanthine (Sigma, H9377) and 25 µg/L gentamicin (Melford Laboratories, G38000-1), supplemented with 5 g/L Albumax II (Invitrogen, 11021037), 10% horse serum (Gibco, 10368902) and 4 g/L glucose for *P. knowlesi*, or with 2.5 g/L Albumax II and 5% human serum for *P. falciparum*. *P. falciparum* and *P. knowlesi* were cultured in human red blood cells (NHS Blood and Transplant) at 4% or 2% haematocrit respectively in 3% oxygen, 5% CO_2 and 92% nitrogen gas mixture at 37°C.

For *P. falciparum* synchronization, parasites at ~ 6% parasitaemia were initially synchronised with 5% sorbitol (w/v in water) and allowed to grow to late schizont stage. ML-10 (LifeArc) (Large, Birchall et al. 2019, Large, Birchall et al. 2019) was then added for 2h

at a final concentration of 75 nM. Schizonts were purified via a 65% Percoll (GE Healthcare) gradient (v/v in PBS), washed twice with complete media, and allowed to reinvade in 25% haematocrit in 5 ml of complete media in the abovementioned gas mixture at 37°C for 3h with agitation at 220 rpm. 5% sorbitol was then used to remove residual schizonts and produce a tightly synchronised culture (0 to 3 hours post invasion (hpi)).

For *P. knowlesi* synchronization, parasites at ~ 6% parasitaemia were centrifuged through a 55% Nycodenz gradient (v/v in RPMI) from 100% Nycodenz stock pH 7.5 (27.6% w/v Nycodenz, 5 mM Tris HCl, 3 mM KCl, 0.3 mM $CaNa_2$·EDTA). Ring stages isolated in the bottom layer were allowed to grow to late schizont stage. ML-10 was then added to a final concentration of 150 nM for 2h. Parasites were centrifuged through a second Nycodenz gradient to collect schizonts from the top layer, which were washed twice with complete media and allowed to reinvade as above. A second Nycodenz cleanup was then performed to remove residual schizonts and produce a tightly synchronised culture (0 to 3 hpi).

Growth of *P. yoelii* and *P. berghei*

Eight-week-old wild-type female C57BL/6J or CD1 mice were obtained from Charles River Laboratories. All mice were specified pathogen-free, housed in groups of five in individually ventilated cages, and provided ad libitum access to food and water. All experimental protocols and procedures were performed in accordance of the UK Animals (Scientific Procedures) Act (PP8697814), and were approved by the Imperial College Animal Welfare and Ethical Review Board *(*for *P. yoelii)* or the University of Cambridge AWERB (for *P. berghei*). The Office of Laboratory Animal Welfare Assurance for the University of Cambridge covers all Public-Health-Service-supported activities involving live vertebrates (no. A5634-01). This study was carried out in compliance with the ARRIVE guidelines (https://arriveguidelines.org/). All studies were in accordance with the Laboratory Animal Science Association's guidelines for good practice. Prior to any experimental interventions, all mice were acclimatized to animal facilities for one week.

P. yoelii (17XL strain) was serially passaged through C57BL/6J mice, following previously described protocols (Georgiadou, Dunican et al. 2022). Blood was collected via aseptic cardiac puncture from infected donor mice under non-recovery isoflurane anesthesia and diluted in sterile phosphate-buffered saline to achieve the desired parasite concentration. Experimental mice were subsequently infected with 10^6 live parasites via intraperitoneal (i.p.) injection.

P. berghei (ANKA 2.34 strain) was maintained by serial passage through CD1 mice as in previously described protocols (Blagborough, Churcher et al. 2013). Experimental mice were pre-treated with 150µl of 6mg/ml phenylhydrazine i.p. three days prior to infection, to induce reticulocytosis. Blood from donor mice at 1-5% parasitaemia was collected by cardiac puncture under non-recovery Ketaset/Rompun anaesthesia and used to infected experimental mice by passage of 150µl blood, i.p..

Tail capillary blood samples were collected to prepare blood smears for parasitemia assessment and lactate measurement. Parasitemia was quantified through microscopy of

thin blood smears stained with 10% Giemsa, following established protocols (Georgiadou, Dunican et al. 2022). Heparinized blood was collected via cardiac puncture under non-recovery anesthesia, into syringes pre-loaded with heparin, and red blood cells were separated from plasma by centrifugation at 4,000g for 10 minutes. Levels of lactate in the cardiac blood of each mouse were immediately measured using the Lactate Pro 2 meter (HAB Direct) for *P. yoelii* experiments, or the L-lactic acid (L-Lactate) assay kit (Megazyme K-LATE) for *P. berghei* experiments. Red blood cells were harvested for parasite histone extraction from ten mice per rodent malaria species, of which seven yielded a viable amount of parasite material when infected with *P. yoelii* 17XL and five yielded an appropriate amount when infected with *P. berghei* ANKA 2.34.

Sodium L-lactate treatment of *P. falciparum* and *P. knowlesi* cultures

For titration experiments, *P. knowlesi* at 12-14 hpi and *P. falciparum* at 24-26 hpi, both at 1% parasitaemia, were treated with 0mM, 5mM, 10mM or 25mM sodium L-lactate (Sigma), for 8h (*P. knowlesi*) and 12h (*P. falciparum*). Subsequently, samples were harvested and crude histone extractions were performed (as described below).

For timecourse experiments, *P. knowlesi* parasites at 12-14 hpi and *P. falciparum* at 24-26 hpi, both at 1% parasitaemia, were treated with 25mM L-lactate for 8h (*P. knowlesi*) and 12h (*P. falciparum*). Samples were harvested at intervals of 2-6 hours from 14-20 hpi for *P. knowlesi* and 24-36 hpi for *P. falciparum*. Lactate was then washed off after 20 hpi (*P. knowlesi*) and 36 hpi (*P. falciparum*), and fresh media was added to parasites. Samples were subsequently harvested at 4-12h intervals from 20 until 42 hpi (for *P. knowlesi*) and 36 to 60 hpi (for *P. falciparum*). After the wash-off, media was changed every time samples were harvested. Crude histone extractions were performed from each sample. Control experiments were also performed in parallel, where no L-lactate was added, under the same conditions described above.

For mass spectrometry on histones from mixed-stage cultures of both species, parasites at a parasitaemia of ~ 6% were washed into fresh media and sodium L-lactate (Sigma), dissolved in incomplete media, was added to a final concentration of 25 mM. For mass spectrometry on histones from trophozoites, *P. falciparum* at 24-26 hpi and *P. knowlesi* at 12-14 hpi were treated with sodium L-lactate for 12 and 9h respectively.

Extraction of *Plasmodium* histones

P. falciparum and *P. knowlesi* cultures were collected by centrifugation at 800 *x g* for 5 minutes, followed by resuspending the pellet in 1.5 volumes 1X PBS. To release parasites from erythrocytes, saponin was added to a final concentration of 0.1% and incubated on ice for 10 minutes, followed by centrifugation at 12,000 *x g* at 4°C for 10 minutes. Parasite pellets were washed three times by adding ice cold 1X PBS (2 volumes of the saponin lysate) followed by centrifugation at 6000 *x g* for 2 minutes.

For *P. yoelii* and *P. berghei,* infected blood obtained by mouse cardiac puncture was placed in 50 mL RPMI HEPES modification media ('schizont media' - no FCS) and spun at 800

xg for 5 minutes, followed by an RPMI wash and centrifugation at the same speed. To remove host leukocytes, blood was passed through Plasmodipur filters (EuroProxima, 8011) using a syringe, followed by washing the filter with RPMI media to elute any remaining blood. The filtration procedure was repeated a second time before collecting the blood pellet by centrifugation at 800 *xg* for 5 minutes. Filtered blood was then mixed with 0.1 % saponin on ice for 15 minutes to release parasites, which were then collected as above.

Parasites from all species were processed either for crude or acid-based histone extraction. For crude histone extraction, parasite cell pellets were lysed by adding 1X RIPA buffer (250 mM Tris-Hcl pH 8.0, 750 mM NaCl, 5% NP-40, 5% sodium deoxycholate, 0.5% SDS, 1mM phenylmethylsulfonyl fluoride, 1X cComplete EDTA-free protease inhibitor cocktail (Roche)) followed by three freeze/thaw cycles on dry ice, 2 minutes each. Laemmli buffer was then added to a final concentration of 1X, boiled at 95 °C for 10 minutes and stored at -80°C for western blot analysis.

For mass spectrometry analysis, nuclei were liberated from parasite cell pellets by gently resuspending the parasite pellet twice in two volumes of hypotonic buffer A (10 mM Tris-HCl (pH 8.0), 3 mM $MgCl_2$, 0.2% v/v Nonidet P-40, 0.25 M sucrose, and a cocktail of EDTA-free protease inhibitors (Roche, 0469313200) followed by centrifugation at 4000 x *g* at 4°C for 10 minutes. The resulting chromatin pellet was then resuspended in two volumes of hypotonic buffer B (10 mM Tris-HCl, pH 8.0, 0.8 M NaCl, 1 mM EDTA [including protease inhibitor cocktail]) and incubated on ice for 10 minutes followed by centrifugation at 4000 x *g* at 4°C for 10 minutes. The chromatin pellet was then resuspended with eight volumes of 0.25 M ice-cold HCl followed by vigorous vortexing and rotation for 2h at 4 °C. Acid-soluble recovered proteins in the supernatant were collected by centrifugation at 12,000 *x g* for 30 minutes at 4 ^{o}C. Histone-containing supernatant was mixed with an equal volume of 30% TCA and incubated overnight rotating at 4 °C, followed by centrifugation at 12,000 *x g* for 15 minutes at 4 ^{o}C to collect the histone-containing pellet. This was then washed with 500 µl of ice-cold acetone and incubated at -20 ^{o}C for 3h, followed by centrifugation at 12,000 *x g* for 15 minutes. Histone pellet was then air-dried and reconstituted in 50 µl ddH_20. Protein concentration was measured using Qubit protein quantification kit (Invitrogen, Q33211). Purity of extracted histones was then assessed by SDS-PAGE on a 15% acrylamide gel stained with Coomassie blue G-250.

Western blotting

Protein extracts were loaded on 15% SDS polyacrylamide gels. For lactate-titration blots, approximately 10 µg and 100 µg were loaded for *P. falciparum* and *P. knowlesi* protein extracts respectively. For timecourse blots, up to 100 µg and 200 µg were loaded for *P. falciparum* and *P. knowlesi* protein extracts respectively. For validation of histone lactylation prior to mass spectrometry, ~ 10 µg of acid-extracted histones were used. Gels were run at 120 V for 3h and transferred to 0.45 µM nitrocellulose membrane (GE healthcare, 10600020). For both chemiluminescent and fluorescent blots, membranes were

blocked in PBS-0.1% Tween 20 containing 5% bovine serum albumin, then probed with designated primary antibodies. For chemiluminescent detection, horseradish peroxidase (HRP)-coupled secondary antibodies were used and developed with ECL Plus Western Chemiluminescent HRP Substrate (ThermoScientific, 11527271). For fluorescent detection, fluorescent secondary antibodies were used. Blots were imaged with an Azure biosystems imager 500 and densitometry was performed with ImageJ for all western blots from titration and timecourse experiments. All lactylated histone signals were normalised using a parallel blot for total histone H4 (except for fluorescence blots, where lactylated histones were normalized using the H4 signal on the same blot).

Antibodies used in western blotting and immunofluorescence microscopy

Primary antibody	**Dilutions**		**Secondary antibody**	**Dilutions**	
	WB	IF		WB	IF
HA - Anti-HA High Affinity Rat mAB 50 ug (Roche 11867423001)		1:500	Alexa Fluor 488-conjugated anti-rat IgG (ThermoFisher A-11006)		1:1000
KLA - Anti-L-Lactyllysine Rabbit mAb 100 ul (PTM-1401)	1:1000 (chemi) 1:10,000 (fluor)	1:500	Alexa Fluor 594-conjugated anti-rabbit IgG (ThermoFisher A-11012) Goat-anti-rabbit IgG IR800 (AzureSpectra, AC2134)	1:10,000	1:1000
H4KL12 - Anti-Lactyl-Histone H4 (Lys12) Rabbit pAB 100 ul (HOLZEL PTM-1411)	1:000	1:500	Alexa Fluor 594-conjugated anti-rabbit IgG (ThermoFisher A-11012)		1:1000
H3ac - Ant-Histone H3ac (pan-acetyl) Rabbit pAb 100 µg (Active motif 61637)	1:4000	1:500	Alexa Fluor 594-conjugated anti-rabbit IgG (ThermoFisher A-11012)		1:1000
H4ac - Anti-Histone H4 (acetyl K5 + K8 + K12) 50 µg (Abcam ab233193)	1:4000	1:500	Alexa Fluor 594-conjugated anti-rabbit IgG (ThermoFisher A-11012)		1:1000
Rabbit anti-histone H4 (Abcam, ab10158)	1:3000	1:500	HRP-conjugated goat anti-rabbit IgG (Abcam, ab6721)	1:2500	1:1000
Mouse anti-histone H4 (Abcam, ab17036)	1:1000 (fluor)		Goat-anti-mouse IgG IR700 (AzureSpectra, AC2129)	1:10,000	

Lactate assay

Lactate assays were performed using the L-lactic acid (L-Lactate) assay kit (Megazyme K-LATE). Media samples were taken from 5 ml cultures of *P. falciparum* NF54 and *P. knowlesi* A1-H.1, synchronised with Percoll at the ring stage, starting with 0.5% parasitaemia, every 24 h for 5 days. For two biological repeats the cultures were split every 48 h and for another two biological repeats the cultures were not split. The lactate assay was performed according to the manufacturer's instructions (Megazyme K-LATE) on triplicate media samples of 2µl, plated in the 96-well format. The assays were read on a FLUOstar Microplate Reader (BMG LABTECH). Parasitaemia was verified by microscopy every time samples were collected. Results were analysed using GraphPad Prism.

Immunofluorescence assay

Smears were made from *P. falciparum* 3D7 HP1_HA + BSD (gift from Prof Till Voss (Flueck, Bartfai et al. 2009)) and NF54, using mixed stage cultures at 4% parasitaemia. Smears were air dried, fixed in 4% paraformaldehyde/PBS for 10 minutes, washed in PBS, air dried and stored at 4°C. Parasites were permeabilised in 0.2% Triton X-100 for 15 minutes, washed in PBS, and blocked in 1% BSA/PBS with 0.1% Tween-20 for 1 h. Primary antibody labelling was done for 1 h, diluted 1:500 in 1% BSA/PBS, followed by three 5-minute washes with block (1% BSA with 0.1% Tween-20). Secondary antibody labelling was done for 1 h, diluted 1:1000 in 1% BSA/PBS, followed by one 5-minute wash with block (see table 1 for antibodies). The slides were then incubated with DAPI (4'6-diamidino-2-phenylindole) (Thermo Fisher Scientific) at 2 µg/mL in PBS for 5 minutes, followed by one 5-minute wash with block. All incubation and labelling steps were done at room temperature. Slides were cured using ProLong Diamond Antifade Mountant (Invitrogen) at room temperature and stored at 4°C prior to visualisation. Slides were imaged using a confocal fluorescence microscope Zeiss LSM700. Images were pseudo-coloured and merged using Fiji-win64 (Image J).

Mass spectrometry

- <u>Sample preparation for mass spectrometry</u>

50 µg of acid-extracted histones were resolved on SDS-PAGE 15% acrylamide gel (95 V, 3 h). Gel was stained with QC colloidal Coomassie blue G-250 (Biorad, 1610803) for 3 h, then washed with several changes of nuclease-free water over 1 h. Bands between 10 and 15 kDa were then excised and washed with several changes of 50% acetonitrile for destaining, followed by 100% acetonitrile. Gel plugs were then incubated in 0.05 M NH_4HCO_3 and 10 mM DTT at 56 °C for 45 minutes for disulphide bond reduction, and with 55 mM iodoacetamide and 0.1 M NH_4 for alkylation, followed by treatment with iodoacetamide for 30 min at 30 °C in the dark. Gel plugs were then washed with water and 50% acetonitrile. For dehydration, 100% acetonitrile was added, followed by rehydration in 50 mM NH_4HCO_3

containing 12.5 ng/µL trypsin (Promega modified trypsin). Samples were incubated overnight at 37 °C. After digestion, the supernatant was pipetted into a sample vial and loaded onto an autosampler for automated LC-MS/MS analysis.

- Reverse phase chromatography and mass spectrometry

All LC-MS/MS experiments were performed using a Dionex Ultimate 3000 RSLC nanoUPLC system (Thermo Fisher Scientific Inc, Waltham, MA, USA) and a Q Exactive Orbitrap mass spectrometer (Thermo Fisher Scientific Inc, Waltham, MA, USA). Separation of peptides was performed by reverse-phase chromatography at a flow rate of 300 nL/min and a Thermo Scientific reverse-phase nano Easy-spray column (Thermo Scientific PepMap C18, 2mm particle size, 100A pore size, 75 mm i.d. x 50cm length). Peptides were loaded onto a pre-column (Thermo Scientific PepMap 100 C18, 5mm particle size, 100A pore size, 300 mm i.d. x 5mm length) from the Ultimate 3000 autosampler with 0.1% formic acid for 3 minutes at a flow rate of 15 mL/min. After this period, the column valve was switched to allow elution of peptides from the pre-column onto the analytical column. Solvent A was water + 0.1% formic acid and solvent B was 80% acetonitrile, 20% water + 0.1% formic acid. The linear gradient employed was 2-40% B in 90 minutes. Further wash and equilibration steps gave a total run time of 120 minutes.

The LC eluant was sprayed into the mass spectrometer by means of an Easy-Spray source (Thermo Fisher Scientific Inc.). All m/z values of eluting ions were measured in an Orbitrap mass analyzer, set at a resolution of 35000 and was scanned between m/z 380-1500. Data dependent scans (Top 20) were employed to automatically isolate and generate fragment ions by higher energy collisional dissociation (HCD, NCE:26%) in the HCD collision cell and measurement of the resulting fragment ions was performed in the orbitrap analyser, set at a resolution of 17500. Singly charged ions and ions with unassigned charge states were excluded from being selected for MS/MS and a dynamic exclusion window of 40 was employed.

- Data processing, protein quantification and PTM localisation

For all experiments, raw mass spectrometry data were analyzed using MaxQuant (Cox and Mann 2008) v. 1.5.0.0 by employing Andromeda for MS/MS spectra search against the *P. falciparum* and *P. knowlesi* PlasmoDB FASTA proteome reference (release 64), and a common contaminant database (Cox, Neuhauser et al. 2011). In MaxQuant, enzyme specificity was set to Trypsin/P; carbamylation of cysteines was set as a fixed modification and Acetyl lysine, lactyl lysine, and di/tri methyl lysine, as variable modifications. Missed cleavage sites were set to 5 with a maximum number of 3 modifications per peptide. For protein quantification, major protein aggregation was changed to sum. Match between run was turned on. PTMs quantification files generated by MaxQuant were exported to Perseus (v3.6.2) (Tyanova, Temu et al. 2016) to collapse localisation site information and remove reverse and contaminants. For all PTMs, sites identified in both conditions for mixed-stage

experiments, or in at least two replicates per condition for trophozoites. Remaining protein quantification and PTM quantification steps were performed in R (v3.6.2) as described below.

- Downstream data analysis for differential protein and PTM expression

For all experiments, PTM peptide quantification files obtained after Perseus filtering steps described above, and ProteinGroup.txt protein quantification files obtained by MaxQuant, were exported to R for further processing. For mixed-stage experiments, log_2 transformed PTM intensities were normalised using quantile normalisation using the normalizeBetweenArrays function from limma package (v3.42) (Ritchie, Phipson et al. 2015). For trophozoite-stage experiments, log_2 transformed PTM intensities were normalised using quantile and VSN normalisation for *P. falciparum* and *P. knowlesi*, respectively, using the normalizeBetweenArrays function from limma package (v3.42). VSN was chosen for the latter due to technical variability between biological replicates, which affected replicate 1 only from both + and - lactate conditions. Imputation of missing values was done by low-rank approximation of the normalised PTM data matrix using msImpute (Hediyeh-Zadeh, Webb et al. 2023). In brief, imputation was performed with V2 method if values were missing at random, or by Barycenter approach if missingness was not at random. Differentially expressed sites were calculated using limma (two-sided, BH p value < 5%). At the protein level, reverse and contaminants were removed from ProteinGroup.txt quantification file, followed by extracting LFQ intensities and requiring at least two values per condition. For better accuracy in global protein levels, spectraCounteBayes function from DEqMS package (v1.22.0) (Zhu, Orre et al. 2020) was used to make limma's empirical-Bayesian variance calculation dependent on the number of detected peptides/PTMs per protein generated by MaxQuant, rather than estimating a fixed prior distribution for all proteins. Finally, differentially expressed proteins were calculated using limma (two-sided, BH FDR < 1%).

RNA-seq data analysis

Raw reads from the RNA-Seq experiment generated by (Georgiadou, Dunican et al. 2022), belonging to Py17XL and PbANKA early and late infection stages, were downloaded, trimmed and quality checked by Trimmomatic v.0.35 (Bolger, Lohse et al. 2014). Low quality reads with Phred quality score values lower than 30 and lengths less than 20 bp were removed. (https://www.bioinformatics.babraham.ac.uk/projects/fastqc/). Filtered reads were further quality controlled by FastQC v.0.11.7 (https://www.bioinformatics.babraham.ac.uk/projects/fastqc/)) and used for transcript quantification using SALMON v.0.82 (Patro, Duggal et al. 2017). Py17XL and PbANKA reference transcript datasets were indexed using the quasi-mapping mode (--type quasi) of Salmon to create k-mers of lengths 31 (-K 31). For transcript quantification, input data sequence bias correction and bootstrapped abundance estimate were performed using the "seqBias" and "nom-Bootstraps 30" parameters from Salmon, respectively. Read counts

and transcript per million reads (TPMs) were generated using tximport R package version 1.10.0 and lengthScaledTPM method (Soneson, Matthes et al. 2016) with inputs of transcript quantifications from tool SALMON. Low-expressed transcripts and genes were filtered based on analysing the data mean-variance trend. The expected decreasing trend between data mean and variance was observed when expressed transcripts were determined as those that had 3 of the 6 samples with count per million reads (CPM) 1, which provided an optimal filter for low expression. A gene was considered to be expressed if any of its transcripts with the above criteria was expressed. The TMM method was used to normalise the gene and transcript read counts to –CPM (Bullard, Purdom et al. 2010).

Prior to DE analysis and to control for heterogeneity within parasite developmental stages, we performed parasite stage deconvolution as follows. A signature matrix was taken from (Tebben, Dia et al. 2022), which contains CPM-normalised gene expression measurements calculated across different parasite stages (male and female gametocyte, trophozoite, ring, merozoite, and schizont stages). *P. berghei* and *P. yoelii* gene names were converted to one-to-one orthologous *P. falciparum* gene names using an orthologous gene file obtained from the Malaria Cell Atlas. CPM-normalised counts alongside the signature matrix were then uploaded to CIBERSORT for deconvolution analysis using 100 permutations and disabling quantile normalisation (as recommended by CIBERSORT) to obtain the parasites cell proportions. This was performed separately for reads mapping to *P. berghei* and *P. yoelii*.

For DE analysis, limma suite was used (Law, Chen et al. 2014, Ritchie, Phipson et al. 2015) by fitting a linear model accounting for the cell proportions obtained in CIBERSORT. To compare the expression changes between conditions of experimental design, the contrast groups were set as Late-Early. For DE genes/transcript, the fold change of gene/transcript abundance were calculated based on contrast groups and significance of expression changes were determined using t-test. P-values of multiple testing were adjusted with BH to correct false discovery rate (FDR) (Benjamini and Yekutieli 2005). A gene/transcript was considered significantly DE in a contrast group if it had adjusted p-value < 0.01 and $|\log2FC| \geq 1$.

Gene ontology (GO) pathway enrichment analysis

For RNA-Seq datasets, functional GO and pathway enrichment analysis were performed on significantly DE genes only, using PlasmoDB database (Aurrecoechea, Brestelli et al. 2009) for annotation with default parameters. The GO terms (biological process, molecular function and cellular component) and pathways were identified to provide biological insights into the significance of DE using a *P-value* ≤ 0.05. For visualization of GO and pathways terms, combined with their associated gene expression profiles/significance, GOPlot R package v.1.02 was used (Walter, Sanchez-Cabo et al. 2015).

For mass-spectrometry, functional GO enrichment analysis was performed using PlasmoDB database for annotation, with default parameters, on significantly differential proteins of the acid-extracted proteome and PTMs (for the trophozoite-stage experiment

only). Exceptionally, for the KLa PTM, GO enrichment analysis was performed on both significantly and non-significantly changing lactylated proteins. Bubble plots were generated using GO terms combined with their associated genes expression profiles/significance across all PTMs and the acid-extracted proteome via in-house R scripts. For both datasets,

$$\text{Z-score} = \frac{(Up-Down)}{\sqrt{Count}}$$

Where *up* and *down* are the number of genes up-regulated (logFC>0) in the data or down-regulated (logFC<0), respectively.

ACKNOWLEDGEMENTS

We acknowledge the Cambridge Centre for Proteomics for mass spectrometry; the staff of Imperial College Central Biomedical Services for support with animal experiments; Till Voss (Swiss TPH) for the HP1-HA parasite line; and Rachana Ramarao and Anders Jensen for early work on this project.

FUNDING

This work was funded by Wellcome Discovery Award 225171/Z/22/Z to CJM.
AG is supported by an Imperial College Research Fellowship.
AMB is funded by the MRC [MR/N00227×/1 and MR/W025701/1], Sir Isaac Newton Trust, Alborada Fund, Wellcome Trust ISSF and University of Cambridge JRG Scheme, GHIT, Rosetrees Trust (G109130) and the Royal Society (RGS/R1/201,293 and IEC/R3/19,302).

REFERENCES

Andrade, C. M., H. Fleckenstein, R. Thomson-Luque, S. Doumbo, N. F. Lima, C. Anderson, J. Hibbert, C. S. Hopp, T. M. Tran, S. Li, M. Niangaly, H. Cisse, D. Doumtabe, J. Skinner, D. Sturdevant, S. Ricklefs, K. Virtaneva, M. Asghar, M. V. Homann, L. Turner, J. Martins, E. L. Allman, M. E. N'Dri, V. Winkler, M. Llinas, C. Lavazec, C. Martens, A. Farnert, K. Kayentao, A. Ongoiba, T. Lavstsen, N. S. Osorio, T. D. Otto, M. Recker, B. Traore, P. D. Crompton and S. Portugal (2020). "Increased circulation time of Plasmodium falciparum underlies persistent asymptomatic infection in the dry season." Nat Med **26**(12): 1929-1940.

Aurrecoechea, C., J. Brestelli, B. P. Brunk, J. Dommer, S. Fischer, B. Gajria, X. Gao, A. Gingle, G. Grant, O. S. Harb, M. Heiges, F. Innamorato, J. Iodice, J. C. Kissinger, E. Kraemer, W. Li, J. A. Miller, V. Nayak, C. Pennington, D. F. Pinney, D. S. Roos, C. Ross, C. J. Stoeckert, Jr., C. Treatman and H. Wang (2009). "PlasmoDB: a functional genomic database for malaria parasites." Nucleic Acids Res **37**(Database issue): D539-543.

Babbitt, S. E., L. Altenhofen, S. A. Cobbold, E. S. Istvan, C. Fennell, C. Doerig, M. Llinas and D. E. Goldberg (2012). "Plasmodium falciparum responds to amino acid starvation by entering into a hibernatory state." Proc Natl Acad Sci U S A **109**(47): E3278-3287.

Barber, B. E., M. J. Grigg, T. William, T. W. Yeo and N. M. Anstey (2017). "The Treatment of Plasmodium knowlesi Malaria." Trends Parasitol **33**(3): 242-253.

Benjamini, Y. and D. Yekutieli (2005). "Quantitative trait Loci analysis using the false discovery rate." Genetics **171**(2): 783-790.

Blagborough, A. M., T. S. Churcher, L. M. Upton, A. C. Ghani, P. W. Gething and R. E. Sinden (2013). "Transmission-blocking interventions eliminate malaria from laboratory populations." Nat Commun **4**: 1812.
Bolger, A. M., M. Lohse and B. Usadel (2014). "Trimmomatic: a flexible trimmer for Illumina sequence data." Bioinformatics **30**(15): 2114-2120.
Bullard, J. H., E. Purdom, K. D. Hansen and S. Dudoit (2010). "Evaluation of statistical methods for normalization and differential expression in mRNA-Seq experiments." BMC Bioinformatics **11**: 94.
Calixto, C. P. G., W. Guo, A. B. James, N. A. Tzioutziou, J. C. Entizne, P. E. Panter, H. Knight, H. G. Nimmo, R. Zhang and J. W. S. Brown (2018). "Rapid and Dynamic Alternative Splicing Impacts the Arabidopsis Cold Response Transcriptome." Plant Cell **30**(7): 1424-1444.
Cox, J. and M. Mann (2008). "MaxQuant enables high peptide identification rates, individualized p.p.b.-range mass accuracies and proteome-wide protein quantification." Nat Biotechnol **26**(12): 1367-1372.
Cox, J., N. Neuhauser, A. Michalski, R. A. Scheltema, J. V. Olsen and M. Mann (2011). "Andromeda: a peptide search engine integrated into the MaxQuant environment." J Proteome Res **10**(4): 1794-1805.
Dai, E., W. Wang, Y. Li, D. Ye and Y. Li (2024). "Lactate and lactylation: Behind the development of tumors." Cancer Lett **591**: 216896.
Diffendall, G., A. Claës, A. Barcons-Simon, P. Nyarko, F. Dingli, M. Santos, D. Loew, A. Claessens and A. Scherf (2024). "RNA polymerase III is involved in regulating Plasmodium falciparum virulence." eLife **13**(RP95879).
Duraisingh, M. T. and D. Horn (2016). "Epigenetic Regulation of Virulence Gene Expression in Parasitic Protozoa." Cell Host Microbe **19**(5): 629-640.
Flueck, C., R. Bartfai, J. Volz, I. Niederwieser, A. M. Salcedo-Amaya, B. T. Alako, F. Ehlgen, S. A. Ralph, A. F. Cowman, Z. Bozdech, H. G. Stunnenberg and T. S. Voss (2009). "Plasmodium falciparum heterochromatin protein 1 marks genomic loci linked to phenotypic variation of exported virulence factors." PLoS Pathog **5**(9): e1000569.
Georgiadou, A., C. Dunican, P. Soro-Barrio, H. J. Lee, M. Kaforou and A. J. Cunnington (2022). "Comparative transcriptomic analysis reveals translationally relevant processes in mouse models of malaria." Elife **11**.
Harris, C. T., X. Tong, R. Campelo, I. M. Marreiros, L. N. Vanheer, N. Nahiyaan, V. A. Zuzarte-Luis, K. W. Deitsch, M. M. Mota, K. Y. Rhee and B. F. C. Kafsack (2023). "Sexual differentiation in human malaria parasites is regulated by competition between phospholipid metabolism and histone methylation." Nat Microbiol **8**(7): 1280-1292.
Hart, K. J., B. J. Power, K. T. Rios, A. Sebastian and S. E. Lindner (2021). "The Plasmodium NOT1-G paralogue is an essential regulator of sexual stage maturation and parasite transmission." PLoS Biol **19**(10): e3001434.
Hediyeh-Zadeh, S., A. I. Webb and M. J. Davis (2023). "MsImpute: Estimation of Missing Peptide Intensity Data in Label-Free Quantitative Mass Spectrometry." Mol Cell Proteomics **22**(8): 100558.
Hikosaka, K., M. Hirai, K. Komatsuya, Y. Ono and K. Kita (2015). "Lactate retards the development of erythrocytic stages of the human malaria parasite Plasmodium falciparum." Parasitol Int **64**(3): 301-303.
Ju, J., H. Zhang, M. Lin, Z. Yan, L. An, Z. Cao, D. Geng, J. Yue, Y. Tang, L. Tian, F. Chen, Y. Han, W. Wang, S. Zhao, S. Jiao and Z. Zhou (2024). "The alanyl-tRNA synthetase AARS1 moonlights as a lactyltransferase to promote YAP signaling in gastric cancer." J Clin Invest **134**(10).
Krishna, S., D. W. Waller, F. ter Kuile, D. Kwiatkowski, J. Crawley, C. F. Craddock, F. Nosten, D. Chapman, D. Brewster, P. A. Holloway and et al. (1994). "Lactic acidosis and hypoglycaemia in children with severe malaria: pathophysiological and prognostic significance." Trans R Soc Trop Med Hyg **88**(1): 67-73.
Large, J. M., K. Birchall, N. S. Bouloc, A. T. Merritt, E. Smiljanic-Hurley, D. J. Tsagris, M. C. Wheldon, K. H. Ansell, P. J. Coombs, C. A. Kettleborough, D. Whalley, L. B. Stewart, P. W. Bowyer, D. A. Baker and

S. A. Osborne (2019). "Potent bicyclic inhibitors of malarial cGMP-dependent protein kinase: approaches to combining improvements in cell potency, selectivity and structural novelty." Bioorg Med Chem Lett **29**(19): 126610.
Large, J. M., K. Birchall, N. S. Bouloc, A. T. Merritt, E. Smiljanic-Hurley, D. J. Tsagris, M. C. Wheldon, K. H. Ansell, P. J. Coombs, C. A. Kettleborough, D. Whalley, L. B. Stewart, P. W. Bowyer, D. A. Baker and S. A. Osborne (2019). "Potent inhibitors of malarial P. Falciparum protein kinase G: Improving the cell activity of a series of imidazopyridines." Bioorg Med Chem Lett **29**(3): 509-514.
Law, C. W., Y. Chen, W. Shi and G. K. Smyth (2014). "voom: Precision weights unlock linear model analysis tools for RNA-seq read counts." Genome Biol **15**(2): R29.
Mancio-Silva, L., K. Slavic, M. T. Grilo Ruivo, A. R. Grosso, K. K. Modrzynska, I. M. Vera, J. Sales-Dias, A. R. Gomes, C. R. MacPherson, P. Crozet, M. Adamo, E. Baena-Gonzalez, R. Tewari, M. Llinas, O. Billker and M. M. Mota (2017). "Nutrient sensing modulates malaria parasite virulence." Nature **547**(7662): 213-216.
Merrick, C. J. (2023). "Histone lactylation: a new epigenetic axis for host-parasite signalling in malaria?" Trends Parasitol **39**(1): 12-16.
Merrick, C. J., C. Huttenhower, C. Buckee, A. Amambua-Ngwa, N. Gomez-Escobar, M. Walther, D. J. Conway and M. T. Duraisingh (2012). "Epigenetic dysregulation of virulence gene expression in severe Plasmodium falciparum malaria." J Infect Dis **205**(10): 1593-1600.
Patro, R., G. Duggal, M. I. Love, R. A. Irizarry and C. Kingsford (2017). "Salmon provides fast and bias-aware quantification of transcript expression." Nat Methods **14**(4): 417-419.
Possemiers, H., L. Vandermosten and P. E. Van den Steen (2021). "Etiology of lactic acidosis in malaria." PLoS Pathog **17**(1): e1009122.
Ritchie, M. E., B. Phipson, D. Wu, Y. Hu, C. W. Law, W. Shi and G. K. Smyth (2015). "limma powers differential expression analyses for RNA-sequencing and microarray studies." Nucleic Acids Res **43**(7): e47.
Soneson, C., K. L. Matthes, M. Nowicka, C. W. Law and M. D. Robinson (2016). "Isoform prefiltering improves performance of count-based methods for analysis of differential transcript usage." Genome Biol **17**: 12.
Su, J., Z. Zheng, C. Bian, S. Chang, J. Bao, H. Yu, Y. Xin and X. Jiang (2023). "Functions and mechanisms of lactylation in carcinogenesis and immunosuppression." Front Immunol **14**: 1253064.
Tebben, K., A. Dia and D. Serre (2022). "Determination of the Stage Composition of Plasmodium Infections from Bulk Gene Expression Data." mSystems **7**(4): e0025822.
Trelle, M. B., A. M. Salcedo-Amaya, A. M. Cohen, H. G. Stunnenberg and O. N. Jensen (2009). "Global histone analysis by mass spectrometry reveals a high content of acetylated lysine residues in the malaria parasite Plasmodium falciparum." J Proteome Res **8**(7): 3439-3450.
Tyanova, S., T. Temu, P. Sinitcyn, A. Carlson, M. Y. Hein, T. Geiger, M. Mann and J. Cox (2016). "The Perseus computational platform for comprehensive analysis of (prote)omics data." Nat Methods **13**(9): 731-740.
Walter, W., F. Sanchez-Cabo and M. Ricote (2015). "GOplot: an R package for visually combining expression data with functional analysis." Bioinformatics **31**(17): 2912-2914.
West, R. and D. J. Sullivan (2020). "Lactic acid supplementation increases quantity and quality of gametocytes in Plasmodium falciparum culture." Infect Immun **15**(89(1)): e00635-00620.
Zhang, D., Z. Tang, H. Huang, G. Zhou, C. Cui, Y. Weng, W. Liu, S. Kim, S. Lee, M. Perez-Neut, J. Ding, D. Czyz, R. Hu, Z. Ye, M. He, Y. G. Zheng, H. A. Shuman, L. Dai, B. Ren, R. G. Roeder, L. Becker and Y. Zhao (2019). "Metabolic regulation of gene expression by histone lactylation." Nature **574**(7779): 575-580.
Zhu, Y., L. M. Orre, Y. Zhou Tran, G. Mermelekas, H. J. Johansson, A. Malyutina, S. Anders and J. Lehtio (2020). "DEqMS: A Method for Accurate Variance Estimation in Differential Protein Expression Analysis." Mol Cell Proteomics **19**(6): 1047-1057.

Zong, Z., F. Xie, S. Wang, X. Wu, Z. Zhang, B. Yang and F. Zhou (2024). "Alanyl-tRNA synthetase, AARS1, is a lactate sensor and lactyltransferase that lactylates p53 and contributes to tumorigenesis." Cell **187**(10): 2375-2392 e2333.

FIGURE LEGENDS

1. *Plasmodium* histones are inducibly lactylated

A, B: Lysine lactylation was measured in *P. falciparum* parasites grown in different concentrations of L-lactate for 12h. Western blots show 'Pan KLa'(A) and histone H4 K12 lactylation ('H4K12La', (B)), as well as histone H4 as a control. Graphs show quantification of each signal relative to histone H4.

C: Lysine lactylation was measured in *P. knowlesi* parasites grown in different concentrations of L-lactate for 8h, as in (A).

D: Lysine lactylation was measured in *P. yoelii* 17XL parasites exposed to varying levels of lactate in the blood of the host mouse. Western blots show 'Pan KLa' and histone H4 as a control. M1-M7, individual mice; L, ladder. Scatter plot represents Pearson correlation (R^2= 0.56) between histone KLa signal intensities normalized to H4 (*y*-axis) and lactate levels in the blood (*x*-axis) upon parasite collection from the host.

2. Histone lactylation is rapidly inducible and reversible

A,B: Lysine lactylation ('Pan KLa', (A)) and histone H4 K12 lactylation ('H4K12La', (B)) were measured in *P. falciparum* parasites grown either in 25mM L-lactate (+Lac), or in control media without added lactate (Ctrl), for 12h, then washed into fresh media. Samples were taken for western blotting at intervals from 0 to 36h. Stage of the parasite culture is also shown on the x-axis: ET, early trophozoite; MT, mid trophozoite; LT, late trophozoite; S, schizont; R, ring.

C,D: Lysine lactylation ('Pan KLa', (A)) and histone H4 K12 lactylation ('H4K12La', (B)) were measured in *P. knowlesi* parasites grown either in 25mM L-lactate, or in control media without added lactate, for 8h, then washed into fresh media. Samples were taken for western blotting at intervals from 0 to 30h. Stage of the parasite culture is shown on the x-axis as in A.

E,F: Lactate levels and parasitaemias were measured every 24h in cultures of *P. falciparum* (E) and *P. knowlesi* (F), starting at 0.5% parasitaemia, either split back to 0.5% every 48h or not split. Data shown are the mean of biological duplicate experiments.

G: *P. falciparum* parasites were grown without splitting or changing the media for 72h, starting at the early-trophozoite stage and sampling every 12h. Stage of the parasite culture is shown on the x-axis as in A. By 60h, parasite morphology showed that the culture was starting to crash, with dead (D) pyknotic parasites by 72h.

3. Histone acetylation is affected by exposure to high lactate

A,B: Histone 3 lysine acetylation ('H3Kac', (A)) and histone 4 lysine acetylation ('H4Kac', (B)) were measured in *P. falciparum* parasites grown in different concentrations of L-lactate for 12h, as in Figure 1.

C,D: Histone 3 lysine acetylation ('H3Kac', (C)) and histone 4 lysine acetylation ('H4Kac', (D)) were measured in *P. knowlesi* parasites grown in different concentrations of L-lactate for 8h, as in Figure 1.

E,F: Histone 3 lysine acetylation ('H3Kac', (E)) and histone 4 lysine acetylation ('H4Kac', (F)) were measured in *P. falciparum* parasites grown either in 25mM L-lactate, or in control media without added lactate, for 12h, then washed into fresh media, as in figure 2. Samples were taken for western blotting at intervals from 0 to 36h. Stage of the parasite culture is shown on the x-axis: ET, early trophozoite; MT, mid trophozoite; LT, late trophozoite; S, schizont; R, ring.

G,H: Histone 3 lysine acetylation ('H3Kac', (G)) and histone 4 lysine acetylation ('H4Kac', (H)) were measured in *P. knowlesi* parasites grown either in 25mM L-lactate, or in control media without added lactate, for 8h, then washed into fresh media, as in figure 2. Samples were taken for western blotting at intervals from 0 to 30h. Stage of the parasite culture is shown on the x-axis as in E.

4. Histone lactylation is distributed throughout the nucleus

Confocal microscopy images showing the location of lactyl PTMs and of HP1 in *P. falciparum* 3D7 HP1_HA. Lactyl-lysine, red; HP1_HA, green; DAPI, blue. KLa (A) and H4K12La (B) distributions are mostly nuclear, and do not colocalise specifically with HA-tagged HP1. T, trophozoite stage; S, schizont stage. Scale bar (2 µm) applies to all images.

5. Histone lactylation occurs on multiple histone lysine residues in two *Plasmodium* species

A: Sequence alignments of histone tails in *P. falciparum* and *P. knowlesi*, showing in red all KLa sites detected by mass spectrometry (either in trophozoite or mixed-stage cultures, +/- 25mM lactate). Numbers in pink flanking the peptide sequences are residue numbers of the N- and C-termini of the peptides. The tail of histone H2A is not shown because no KLa was detected on this histone.

B: Pie charts representing the distribution of KLa sites from (A), and heatmaps representing normalized intensities of KLa-containing peptides (Z-score transformed). Hierarchical clustering was used to partition the KLa sites into 3 clusters with euclidean distance and ward.D clustering algorithm. The time windows for trophozoite cultures of *P. falciparum* and *P. knowlesi* were 24-26 and 12-14 hpi, respectively.

6. Changes in PTMs on both histones and non-histone proteins are induced by exposure to high lactate

Volcano plots representing (A) histones with differential lysine lactylation (KLa) and acetylation (Kac), in the top panels, and differential tri- or di-methylation (Kme3, Kme2) in the lower panels; (B) non-histone proteins with differential lysine lactylation (KLa).
In all plots, data are from trophozoite cultures of *P. falciparum* or *P. knowlesi*, +/- 25mM lactate treatment. X-axes represent $\log_2$ fold changes (FC) calculated from normalized intensities, and y-axes represent *P*-values. Colored dots represent PTMs that changed significantly after lactate exposure, based on their significance threshold indicated by *P*-value. (Grey dots represent those that did not change significantly.) Symbols for histones and non-histones are hatched and filled circles, respectively. Horizontal and vertical lines represent *P*-value and $\log_2$FC significance thresholds.
In (B), gene name abbreviations in *P. falciparum*, on the left: RNA MT, RNA methyltransferase; Histone AT, Histone acetyltransferase; LSD1, lysine specific histone demethylase; TsaD, TSaD-domain-containing protein; RBP25, RNA binding protein 25; RP L46, Ribosomal protein L46; G3P, glyceradehyde-3-phosphate dehydrogenase.
In *P. knowlesi* on the right: snRNP PRP4, small nuclear ribonucleoprotein; HDAC SAP18, histone deacetylase subunit SAP18; Ser/Thr PK, serine/threonine protein kinase, CCR4-NOT, CCR4-NOT complex; PRP5 helicase, Pre-mRNA-processing ATP-dependent RNA helicase; SET2, SET2 histone methyltransferase.

7. <u>Gene ontology (GO) enrichment analysis of biological processes and cellular components enriched in PTMs after lactate exposure</u>
Charts represent the top 5 GO terms (biological processes (A), cellular components (B)) with the highest P-value for each PTM. Triangles mark the GO terms associated with proteins whose PTMs were upregulated; circles mark those down-regulated. Shapes are color-coded based on the magnitude of the fold change. The size of the shape, represented by Z-score, indicates the magnitude of the likelihood that the term is up- or down-regulated. *P.f* and *P.k* represent *P. falciparum* (all data on the left of the vertical dashed line) and *P. knowlesi* (right of dashed line). For simplicity, K(me3) and K(me2) are both presented as K(me). 'KLa' refers to all KLa sites detected; KLa.Sig refers to lactylated proteins that changed significantly upon lactate exposure in trophozoites.

8. <u>Transcriptomic profiles of rodent malaria parasites in hosts with varying levels of lactataemia</u>

A: Violin plot representing the distribution and number of significantly up- and down-regulated genes (*P*-value ≤0.05) in *P. yoelii* 17XL (orange, on the left) and *P. berghei* ANKA (blue, on the right) in late-stage versus early-stage infection. Violin width is irrespective of data range.

B: Volcano plots representing differentially expressed genes detected in late versus early infections of *P. yoelii* 17XL (top) and *P. berghei* ANKA (bottom). X-axes represent $\log_2$ fold changes (FC) calculated from normalized CPM values; y-axes represent *P*-values. Coloured dots represent DE genes, based on their significance threshold indicated by

adjusted *P*-value (FDR) (purple dots represent those below any significance threshold). Horizontal and vertical dashed lines represent *P*-value and $\log_2$FC significance thresholds. Gene name abbrevations in *P. yoelli*: SP15, transcription elongation factor SPT5; TIFII, eukaryotic translation initiation factor 3 subunit L; HSP20, HSP20-like chaperone; nPrx, peroxiredoxin; PFK11, ATP-dependent 6-phosphofructokinase; H2B, histone H2B; H4, histone H4; SOD2, superoxide dismutase [Fe]; GEST, gamete egress and sporozoite traversal protein; L-LDH, L-lactate dehydrogenase; LDH, lactate dehydrogenase; FD3, female development protein FD3; H2B.Z, Histone H2B variant; MDV1, male development protein 1; FD1, female development protein 1.
Gene name abbrevations in *P. berghei*: ApiAP2, AP2 domain transcription factor; GSK3beta, glycogen synthase kinase-3 beta; GNAT, N-acetyltransferase in GNAT family; MCM2/5/9, DNA replication licensing factor MCM2/5/9; RECQ1, ATP-dependent DNA helicase RecQ1; SET7, histone-lysine N-methyltransferase SET7; G3PDH, glycerol-3-phosphate dehydrogenase; RIP, PIR protein; Sir2A, histone deacetylase Sir2A; CAF1B, chromatin assembly factor 1 subunit B.

C: Heatmaps representing late and early transcriptional profiles in $\log_2$CPM (Z-score transformed) for DE genes (502 in *P. yoelii*, 1521 in *P. berghei*). Hierarchical clustering was performed to cluster genes expression profiles with euclidean distance and ward.D clustering algorithm.

D: Biological process gene ontology (GO) enrichment analysis of DE genes in *P. berghei* and *P. yoelii.* Plots show the top 15 GO terms with the highest *P*-values. The outer circle displays scatterplots of the expression levels ($\log_2$FC) for the genes in each GO term, whereas the inner circle is a bar plot where the height of the bar indicates the significance of the term (−log10 *P*-value). The colour corresponds to the Z-score, which indicates whether the term is likely to be decreased (negative value) or increased (positive value).

SUPPLEMENTARY FIGURE LEGENDS

1. <u>*Plasmodium* histones are inducibly lactylated</u>

A, B: Replicate experiment for Figure 1A,B. Lysine lactylation ('Pan KLa', (A)) and histone H4 K12 lactylation ('H4K12La', (B)) were measured by western blotting in *P. falciparum* parasites grown in different concentrations of L-lactate for 12h, with histone H4 as a control. Graphs show quantification of each signal relative to histone H4.

C, D: Replicate experiment for Figure 1C. Lysine lactylation ('Pan KLa', (A)) and histone H4 K12 lactylation ('H4K12La', (B)) were measured in *P. knowlesi* parasites grown in different concentrations of L-lactate for 8h.

D: Lysine lactylation was measured in *P. berghei* ANKA parasites exposed to varying levels of lactate in the blood of the host mouse. Western blots show 'Pan KLa' and histone H4 as a control. M1-M5, individual mice; L, ladder. Scatter plot represents Pearson correlation

(R^2= 0.06) between histone KLa signal intensities normalized to H4 (*y*-axis) and lactate levels in the blood (*x*-axis) upon parasite collection from host.

2. Histone lactylation is rapidly inducible and reversible

A,B: Replicate experiment for Figure 2A,B. Lysine lactylation ('Pan KLa', (A)) and histone H4 K12 lactylation ('H4K12La', (B)) were measured in *P. falciparum* parasites grown either in 25mM L-lactate, or in control media without added lactate, for 12h, then washed into fresh media. Samples were taken for western blotting at intervals from 0 to 36h. Stage of the parasite culture is shown on the x-axis: ET, early trophozoite; MT, mid trophozoite; LT, late trophozoite; S, schizont; R, ring.

C: Replicate experiment for Figure 2C. Lysine lactylation ('Pan KLa') was measured in *P. knowlesi* parasites grown either in 25mM L-lactate, or in control media without added lactate, for 8h, then washed into fresh media. Samples were taken for western blotting at intervals from 0 to 30h. Stage of the parasite culture is shown on the x-axis as in A.

D: Replicate experiment for Figure 2G. *P. falciparum* parasites were grown without splitting or changing the media for 72h, starting at the early-trophozoite stage and sampling every 12h. Stage of the parasite culture is shown on the x-axis as in A. By 60h, the parasite morphology showed that the culture was starting to crash, with dead (D) pyknotic parasites by 72h.

3. Histone acetylation is affected by exposure to high lactate

Replicate experiments for figures 3A-G.

A,B: Histone 3 lysine acetylation ('H3Kac', (A)) and histone 4 lysine acetylation ('H4Kac', (B)) were measured in *P. falciparum* parasites grown in different concentrations of L-lactate for 12h, as in Figure 1.

C,D: Histone 3 lysine acetylation ('H3Kac', (C)) and histone 4 lysine acetylation ('H4Kac', (D)) were measured in *P. knowlesi* parasites grown in different concentrations of L-lactate for 8h, as in Figure 1.

E,F: Histone 3 lysine acetylation ('H3Kac', (E)) and histone 4 lysine acetylation ('H4Kac', (F)) were measured in *P. falciparum* parasites grown either in 25mM L-lactate, or in control media without added lactate, for 12h, then washed into fresh media. Samples were taken for western blotting at intervals from 0 to 36h. Stage of the parasite culture is shown on the x-axis: ET, early trophozoite; MT, mid trophozoite; LT, late trophozoite; S, schizont; R, ring.

G,H: Histone 3 lysine acetylation ('H3Kac', (G)) and histone 4 lysine acetylation ('H4Kac', (H)) were measured in *P. knowlesi* parasites grown either in 25mM L-lactate, or in control media without added lactate, for 8h, then washed into fresh media. Samples were taken for western blotting at intervals from 0 to 30h. Stage of the parasite culture is shown on the x-axis as in E.

4. Histone lactylation is distributed throughout the nucleus

A: Confocal microscopy images showing the nuclear locations of acetyl histone H4 (H4ac) and of HP1 in *P. falciparum* 3D7 HP1_HA. H4ac, red; HP1_HA, green; DAPI, blue.

B: Confocal microscopy images showing the location of KLa in *P. falciparum* NF54. This confirms that the location is the same as that shown in main figure 4, and is not affected by the tagging of HP1 in the line 3D7 HP1_HA (strain used in main figure 4). KLa, red; DAPI, blue.

C: Images as in (B), showing lactyl-H4K12 in the *P. falciparum* NF54 strain.

D: Images as in (B), showing H4ac in the *P. falciparum* NF54 strain.

Scale bar (2 µm) applies to all images. R, ring stage, T, trophozoite stage; S, schizont stage.

5. <u>Acid based histone extraction: quality control</u>

A: Coomassie-stained gel of ~ 25 µg of acid-extracted histones with (**+**) /without (**-**) lactate (lac) resolved between ~ 10 and 15 kDa. Molecular weight marker (MW) in kDa is indicated to the left. Histones and histone variants names in *Plasmodium* species are indicated to the right.

B: Immunoblots showing differential lysine lactylation of histones from synchronized trophozoites in response to 25 mM lactate in *P. knowlesi* and *P. falciparum* (biological triplicates). In each gel, lanes marked (+) and (-) correspond to ~ 1 ug of acid-extracted histones with or without lactate treatment. H4 is used as a loading control. Quantified signals are displayed to the right, as bar graphs. Bars show the mean band intensity from biological replicates, normalized to H4. Error bars show the standard error of the mean. T-tests were performed to check for significant changes between groups (0 mM versus 25 mM lactate), n=3/group, *** indicates *P*-value < 0.01.

6. <u>Distribution of lysine lactylation: peptide intensities</u>

A) Violin plot representing lactylated peptide intensities detected by mass spectrometry for samples with (Lactate) and without (Control) 25mM lactate treatment, with the middle horizontal line representing the median. The yellow shape shows the distribution of the data, and the grey dots represent the $\log_2$ transformed lactylation values for individual peptides.

B) Venn diagram representing histone lysine (K) sites of *Plasmodium* that can be either uniquely lactylated (KLa) (dark pink), acetylated (Kac) (yellow), or lactylated and acetylated interchangeably (light pink).

7. <u>KLa profiles on histones are more inducible after lactate exposure than other PTMs</u>

A) Heatmap representing normalized intensities of significantly differential PTM sites (Z-score transformed) after 25mM lactate treatment: histone lysine lactylation (KLa), acetylation (Kac), trimethylation (Kme3) and dimethylation (Kme2). Hierarchical clustering was performed for each species, *P. falciparum* and *P. knowlesi,* independently to cluster the PTM site expression profiles with euclidean distance and ward.D clustering algorithm. The colored bar on the left represents the categories of histone PTM (lactyl/acetyl/methyl).

B) Heatmap representing normalized intensities of the few histone Kac sites that were significantly differential, and that can be interchangeably – and significantly differentially – lactylated as well, in response to 25 mM lactate in *P. falciparum*.

8. KLa profiles in the acid-extracted proteome of *P. knowlesi* and *P. falciparum*

A) Heatmap representing normalized peptide intensities of KLa sites on histone (red) and non-histone (black) proteins (Z-score transformed). Data from *P. falciparum* mixed-stage culture, +/-25 mM lactate treatment. Hierarchical clustering was performed to cluster protein expression profiles with euclidean distance and ward.D clustering algorithm.

B) Heatmap representing normalized peptide intensities of KLa sites on histone (red) and non-histone (black) proteins (Z-score transformed). Data from *P. knowlesi* mixed-stage culture, +/-25 mM lactate treatment. Hierarchical clustering was performed to cluster protein expression profiles with euclidean distance and ward.D clustering algorithm.

9. Comparison between the *Plasmodium* proteome and lactate-induced PTM landscape shows little correlation between PTMs and protein abundance

A) Volcano plots representing differential proteome changes in *Plasmodium* trophozoites in response to 25 mM lactate treatment. X-axes represent $\log_2$ fold changes (FC) calculated from normalized intensities, and y-axes represents $-\log_{10}$ transformed scaled adjusted *P*-values, and scaled *P*-values, for *P. falciparum and P. knowlesi*, respectively. Colored dots represent significantly changing proteins, based on their significance threshold indicated by *P*-value. Dashed black horizontal and vertical lines represent *P*-value and $\log_2$FC significance thresholds.

B) Scatter plot representing correlation between significantly changing lactylated peptides and their protein abundance. $\log_2$FC of the lactylated peptide is plotted on the x-axis and the corresponding proteome $\log_2$FC is plotted on the y-axis. Pearson correlation coefficient (Pearson R) between both entities for each *Plasmodium* species is shown in red. Histone and non-histone proteins are in light orange and sky-blue, respectively. The linear regression fit is shown by the green line (*x* and *y* reflect $\log_2$FC on x-axes and y-axes, respectively). Only proteins with 2 unique razor+ peptides were included in the analysis.

10. GO enrichment analysis of biological processes related to PTMs that are influenced by lactate exposure

GO terms are shown for the proteins with significantly differential PTMs, and for proteins that changed significantly in the chromatin-associated proteome, after 25mM lactate treatment. Each GO term is represented with the genes associated with it as up- (triangle) or/and down- (circle) regulated. Shapes are color-coded based on the magnitude of the fold change. The size of the shape, represented by Z-score, indicates whether the term is likely to be decreased (negative value) or increased (positive value). For simplicity, K(me3) and K(me2) are presented as K(me). *P.f* and *P.k* represent Plasmodium *knowlesi* and

falciparum, respectively. KLa.Sig and KLa represent GO terms enrichment for differentially expressed KLa proteins and lactylated acid-extracted proteome, respectively. Dashed vertical lines separate *P. knowlesi* and *P. falciparum* GO enrichment.

11. GO enrichment analysis of cellular components related to PTMs that are influenced by lactate exposure

GO terms are shown for the proteins with significantly differential PTMs, and for proteins that changed significantly in the chromatin-associated proteome, after 25mM lactate treatment. Each GO term is represented with the genes associated with it as up- (triangle) or/and down- (circle) regulated. Shapes are color-coded based on the magnitude of the fold change. The size of the shape, represented by Z-score, indicates whether the term is likely to be decreased (negative value) or increased (positive value). For simplicity, K(me3) and K(me2) are presented as K(me). *P.f* and *P.k* represent Plasmodium *knowlesi* and *falciparum*, respectively. KLa.Sig and KLa represent GO terms enrichment for differentially expressed KLa proteins and lactylated acid-extracted proteome, respectively. Dashed vertical lines separate *P. knowlesi* and *P. falciparum* GO enrichment.

12. GO enrichment analysis of molecular function related to PTMs that are influenced by lactate exposure

GO terms are shown for the proteins with significantly differential PTMs, and for proteins that changed significantly in the chromatin-associated proteome, after 25mM lactate treatment. Each GO term is represented with the genes associated with it as up- (triangle) or/and down- (circle) regulated. Shapes are color-coded based on the magnitude of the fold change. The size of the shape, represented by Z-score, indicates whether the term is likely to be decreased (negative value) or increased (positive value). For simplicity, K(me3) and K(me2) are presented as K(me). *P.f* and *P.k* represent Plasmodium *knowlesi* and *falciparum*, respectively. KLa.Sig and KLa represent GO terms enrichment for differentially expressed KLa proteins and lactylated acid-extracted proteome, respectively. Dashed vertical lines separate *P. knowlesi* and *P. falciparum* GO enrichment.

13. Quality control for differential expression analysis at late versus early stage of infection in *P.yoelii* 17XL and *P.berghei* ANKA

A) Principal component analysis of RNA-Seq gene expression data representing normalized counts of 4983 and 4712 genes from three biological replicates (Rn) corresponding to *P. yoelii* (top panel) and *P. berghei* (bottom panel), respectively, at early (pink), and late (green) stages of mouse infection.

B) Violin plot representing the distribution and number of significantly up- and down-regulated genes (*P*-value ≤0.01 and |log2FC| ≥ 1) in *P. yoelii* 17XL (green) and *P. berghei* ANKA (purple) in late-stage versus early-stage infection . Violin width is irrespective of data range.

14. GO enrichment analysis of genes differentially expressed at late versus early stage of infection in *P.yoelii* 17XL and *P.berghei* ANKA

A) Molecular function gene ontology (GO) enrichment analysis of DE genes in *P. berghei* and *P. yoelii.* Plots show the top 15 GO terms enriched in molecular function.
B) Top 15 GO terms enriched in cellular components of DE genes in *P. berghei* and *P. yoelii*.
C) Top 15 pathways terms enriched in DE genes in *P. berghei* and *P. yoelii*.

For all plots the outer circle displays scatterplots of the expression levels (log2FC) for the genes in each GO term, whereas the inner circle is a bar plot where the height of the bar indicates the significance of the term (−log10 P-value), and color corresponds to the Z-score, which indicates if the term is likely to be decreased (negative value) or increased (positive value).

SUPPLEMENTARY TABLE LEGENDS

Supplementary Table 1. *P. falciparum* trophozoite mass spectrometry and differential expression analysis

Supplementary Table 2. *P. knowlesi* trophozoite mass spectrometry and differential expression analysis

Supplementary Table 3. *P. falciparum* mixed stages mass spectrometry analysis

Supplementary Table 4. *P. knowlesi* mixed stages mass spectrometry analysis

Supplementary Table 5. Gene ontology of differentially expressed PTMs sites and acid-extracted proteome components in *P. falciparum* and *P. knowlesi* trophozoites.

Supplementary Table 6. RNA-Seq analysis and GO enrichment of DE genes in *P. berghei* and *P. yoelii.*

Figure 1

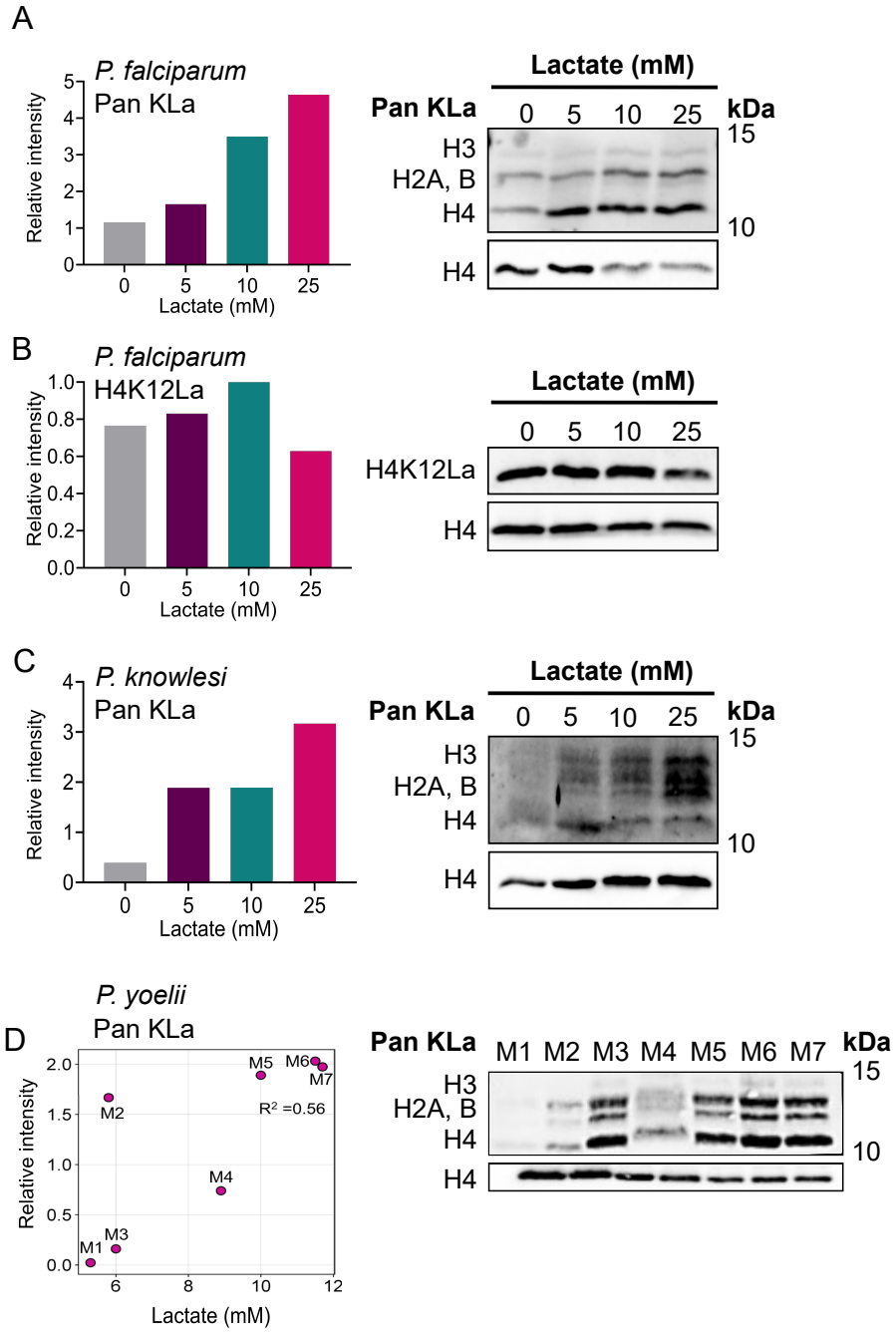
A
P. falciparum
Pan KLa
Relative intensity
Lactate (mM)
Pan KLa
Lactate (mM)
0 5 10 25
kDa
15
10
H3
H2A, B
H4
H4
B
P. falciparum
H4K12La
Relative intensity
Lactate (mM)
Lactate (mM)
0 5 10 25
H4K12La
H4
C
P. knowlesi
Pan KLa
Relative intensity
Lactate (mM)
Pan KLa
Lactate (mM)
0 5 10 25
kDa
15
10
H3
H2A, B
H4
H4
D
P. yoelii
Pan KLa
Relative intensity
Lactate (mM)
M1
M2
M3
M4
M5
M6
M7
R² =0.56
Pan KLa
M1 M2 M3 M4 M5 M6 M7
kDa
15
10
H3
H2A, B
H4
H4

Figure 2

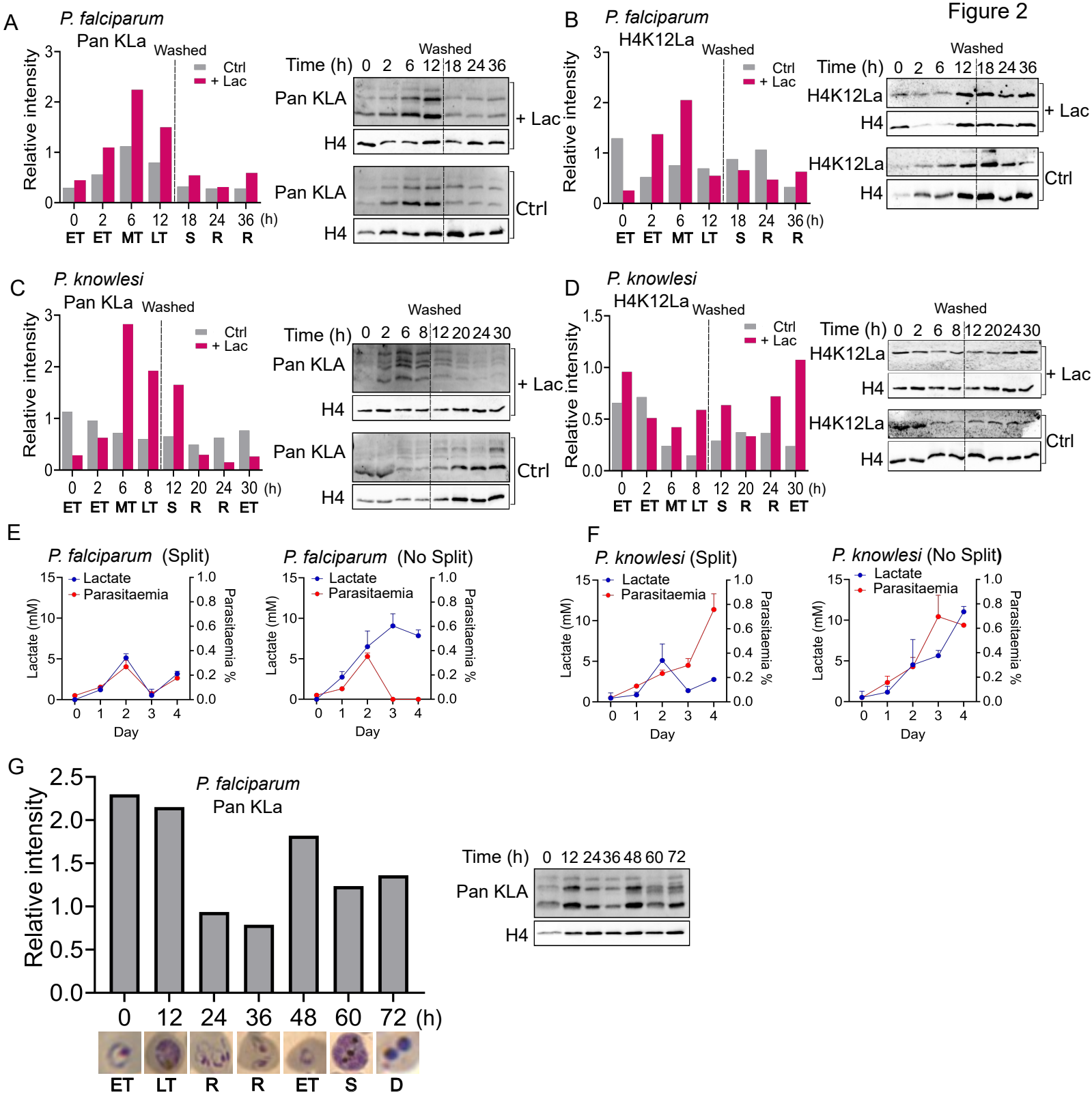
A
P. falciparum
Pan KLa
Washed
Ctrl
+ Lac
Relative intensity
Time (h) 0 2 6 12 18 24 36
Pan KLA
H4
+ Lac
Ctrl
0 2 6 12 18 24 36 (h)
ET ET MT LT S R R
B
P. falciparum
H4K12La
H4K12La
C
P. knowlesi
Pan KLa
Time (h) 0 2 6 8 12 20 24 30
0 2 6 8 12 20 24 30 (h)
ET ET MT LT S R R ET
D
P. knowlesi
H4K12La
E
P. falciparum (Split)
P. falciparum (No Split)
Lactate
Parasitaemia
Lactate (mM)
Parasitaemia %
Day
F
P. knowlesi (Split)
P. knowlesi (No Split)
G
P. falciparum
Pan KLa
Relative intensity
0 12 24 36 48 60 72 (h)
Time (h) 0 12 24 36 48 60 72
Pan KLA
H4
ET LT R R ET S D

Figure 3

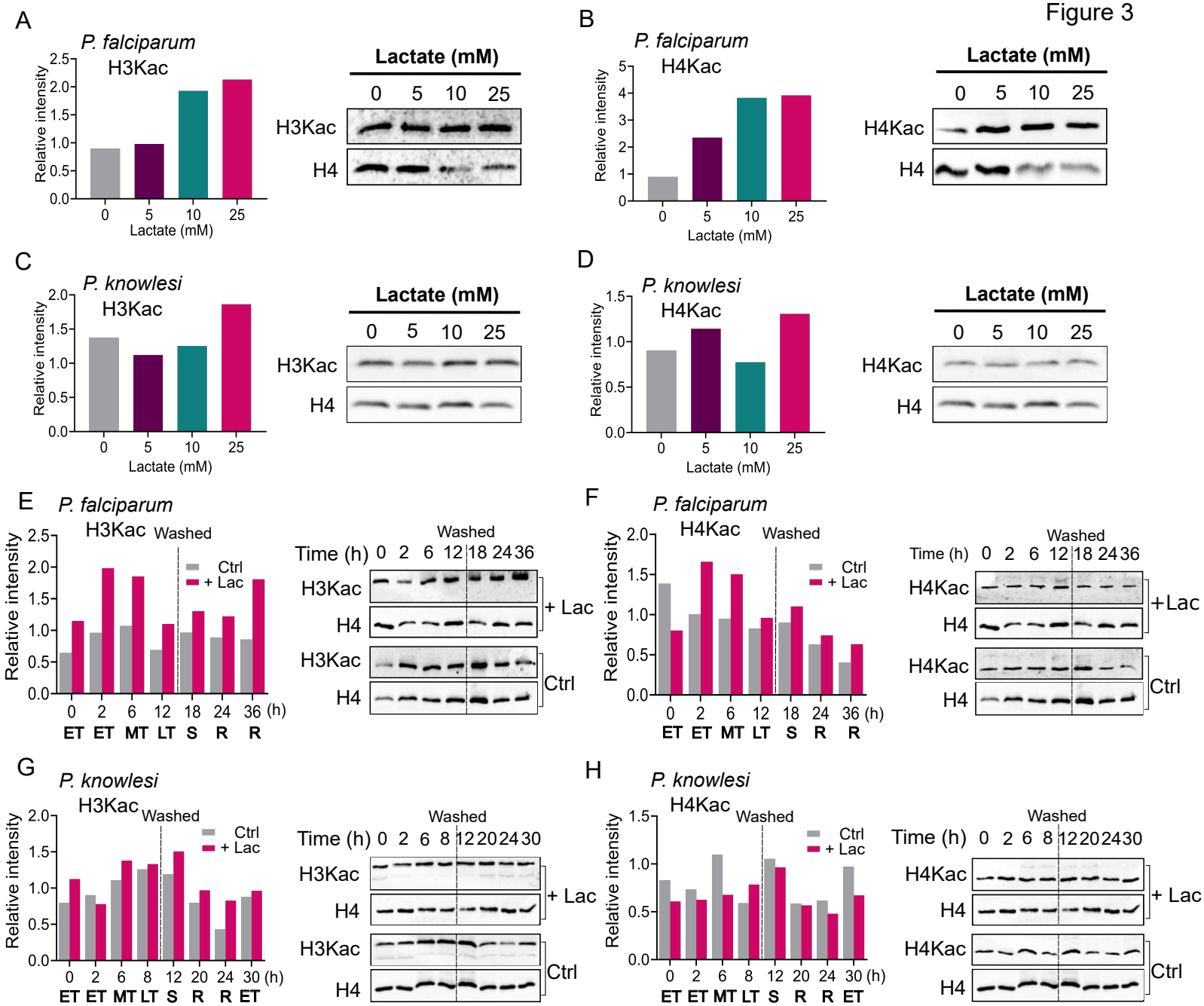
A
P. falciparum
H3Kac
Relative intensity
Lactate (mM)
Lactate (mM)
0 5 10 25
H3Kac
H4
B
P. falciparum
H4Kac
Relative intensity
Lactate (mM)
Lactate (mM)
0 5 10 25
H4Kac
H4
C
P. knowlesi
H3Kac
Relative intensity
Lactate (mM)
Lactate (mM)
0 5 10 25
H3Kac
H4
D
P. knowlesi
H4Kac
Relative intensity
Lactate (mM)
Lactate (mM)
0 5 10 25
H4Kac
H4
E
P. falciparum
H3Kac
Washed
Ctrl
+ Lac
Relative intensity
0 2 6 12 18 24 36 (h)
ET ET MT LT S R R
Washed
Time (h) 0 2 6 12 18 24 36
H3Kac
H4
+ Lac
H3Kac
H4
Ctrl
F
P. falciparum
H4Kac
Washed
Ctrl
+ Lac
Relative intensity
0 2 6 12 18 24 36 (h)
ET ET MT LT S R R
Washed
Time (h) 0 2 6 12 18 24 36
H4Kac
H4
+Lac
H4Kac
H4
Ctrl
G
P. knowlesi
H3Kac
Washed
Ctrl
+ Lac
Relative intensity
0 2 6 8 12 20 24 30 (h)
ET ET MT LT S R R ET
Washed
Time (h) 0 2 6 8 12 20 24 30
H3Kac
H4
+ Lac
H3Kac
H4
Ctrl
H
P. knowlesi
H4Kac
Washed
Ctrl
+ Lac
Relative intensity
0 2 6 8 12 20 24 30 (h)
ET ET MT LT S R R ET
Washed
Time (h) 0 2 6 8 12 20 24 30
H4Kac
H4
+ Lac
H4Kac
H4
Ctrl

Figure 4

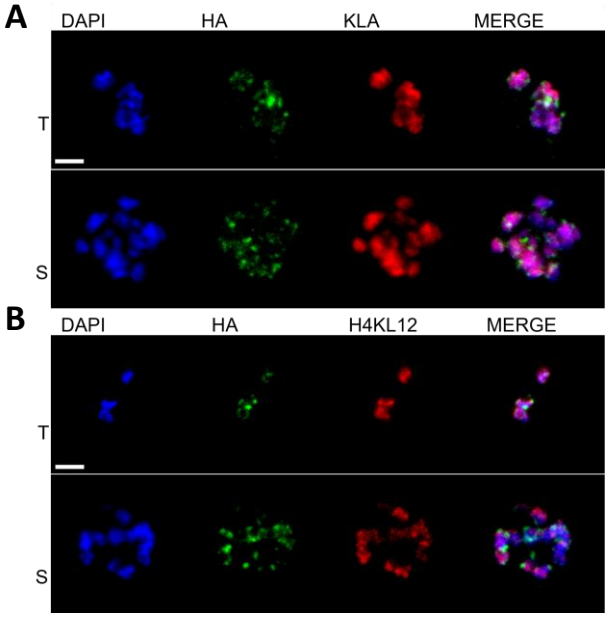

Figure 5

A

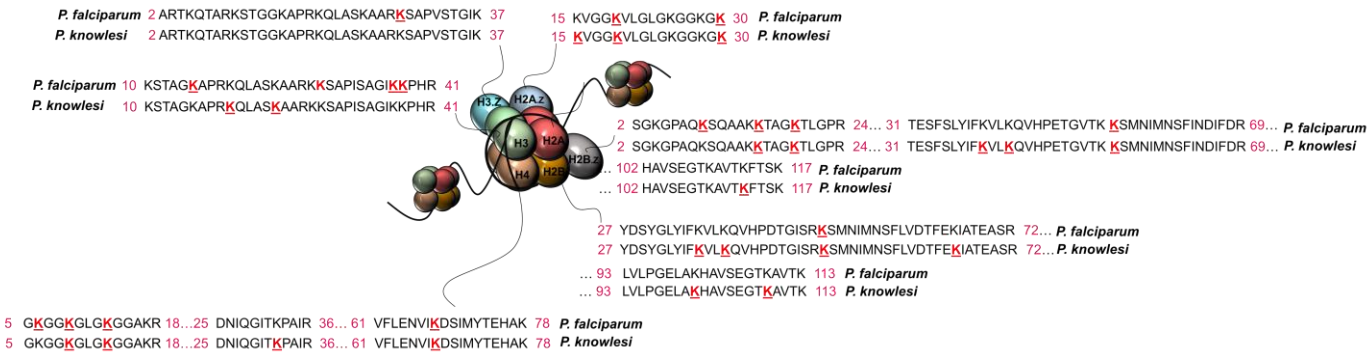
P. falciparum 2 ARTKQTARKSTGGKAPRKQLASKAARKSAPVSTGIK 37
P. knowlesi 2 ARTKQTARKSTGGKAPRKQLASKAARKSAPVSTGIK 37
P. falciparum 10 KSTAGKAPRKQLASKAARKKSAPISAGIKKPHR 41
P. knowlesi 10 KSTAGKAPRKQLASKAARKKSAPISAGIKKPHR 41
15 KVGGKVLGLGKGGKGK 30 P. falciparum
15 KVGGKVLGLGKGGKGK 30 P. knowlesi
2 SGKGPAQKSQAAKKTAGKTLGPR 24... 31 TESFSLYIFKVLKQVHPETGVTK KSMNIMNSFINDIFDR 69... P. falciparum
2 SGKGPAQKSQAAKKTAGKTLGPR 24... 31 TESFSLYIFKVLKQVHPETGVTK KSMNIMNSFINDIFDR 69... P. knowlesi
... 102 HAVSEGTKAVTKFTSK 117 P. falciparum
... 102 HAVSEGTKAVTKFTSK 117 P. knowlesi
27 YDSYGLYIFKVLKQVHPDTGISRKSMNIMNSFLVDTFEKIATEASR 72... P. falciparum
27 YDSYGLYIFKVLKQVHPDTGISRKSMNIMNSFLVDTFEKIATEASR 72... P. knowlesi
... 93 LVLPGELAKHAVSEGTKAVTK 113 P. falciparum
... 93 LVLPGELAKHAVSEGTKAVTK 113 P. knowlesi
5 GKGGKGLGKGGAKR 18...25 DNIQGITKPAIR 36... 61 VFLENVIKDSIMYTEHAK 78 P. falciparum
5 GKGGKGLGKGGAKR 18...25 DNIQGITKPAIR 36... 61 VFLENVIKDSIMYTEHAK 78 P. knowlesi
H3.Z
H2A.Z
H3
H2A
H4
H2B.Z

B

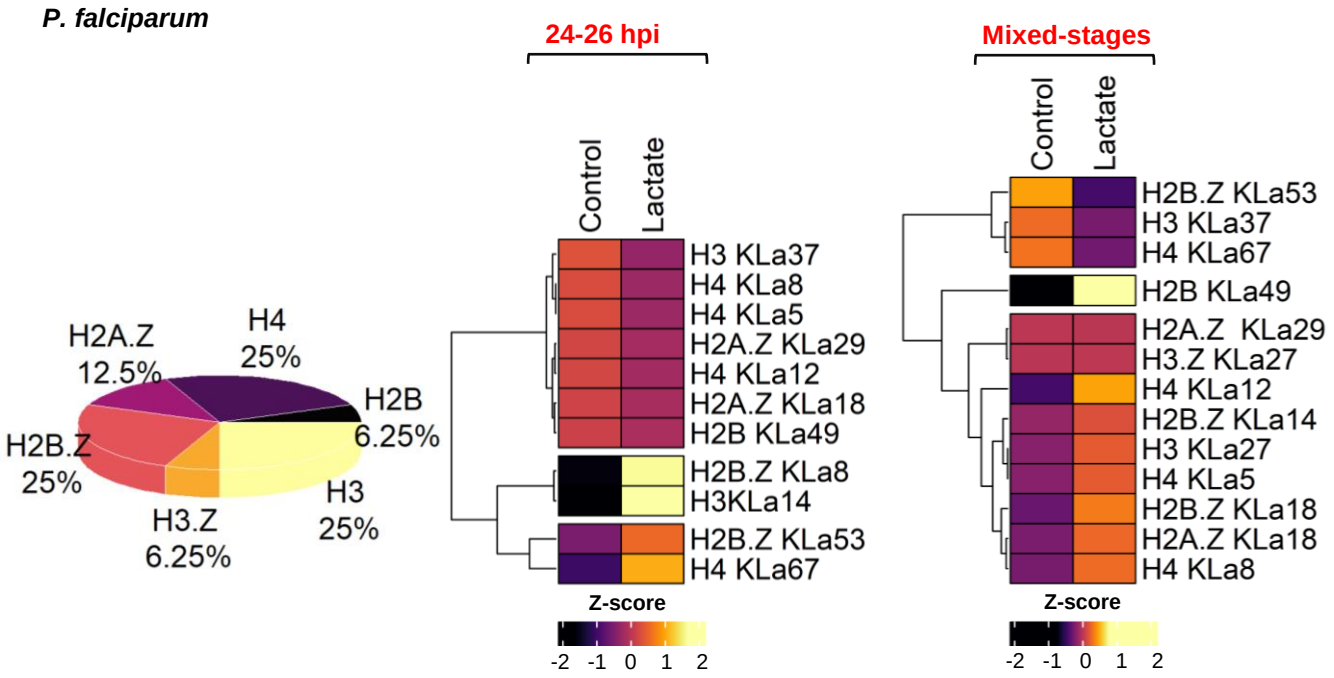
P. falciparum
24-26 hpi
Mixed-stages
Control
Lactate
H2A.Z 12.5%
H4 25%
H2B 6.25%
H2B.Z 25%
H3.Z 6.25%
H3 25%
H3 KLa37
H4 KLa8
H4 KLa5
H2A.Z KLa29
H4 KLa12
H2A.Z KLa18
H2B KLa49
H2B.Z KLa8
H3KLa14
H2B.Z KLa53
H4 KLa67
H2B.Z KLa53
H3 KLa37
H4 KLa67
H2B KLa49
H2A.Z KLa29
H3.Z KLa27
H4 KLa12
H2B.Z KLa14
H3 KLa27
H4 KLa5
H2B.Z KLa18
H2A.Z KLa18
H4 KLa8
Z-score
-2 -1 0 1 2

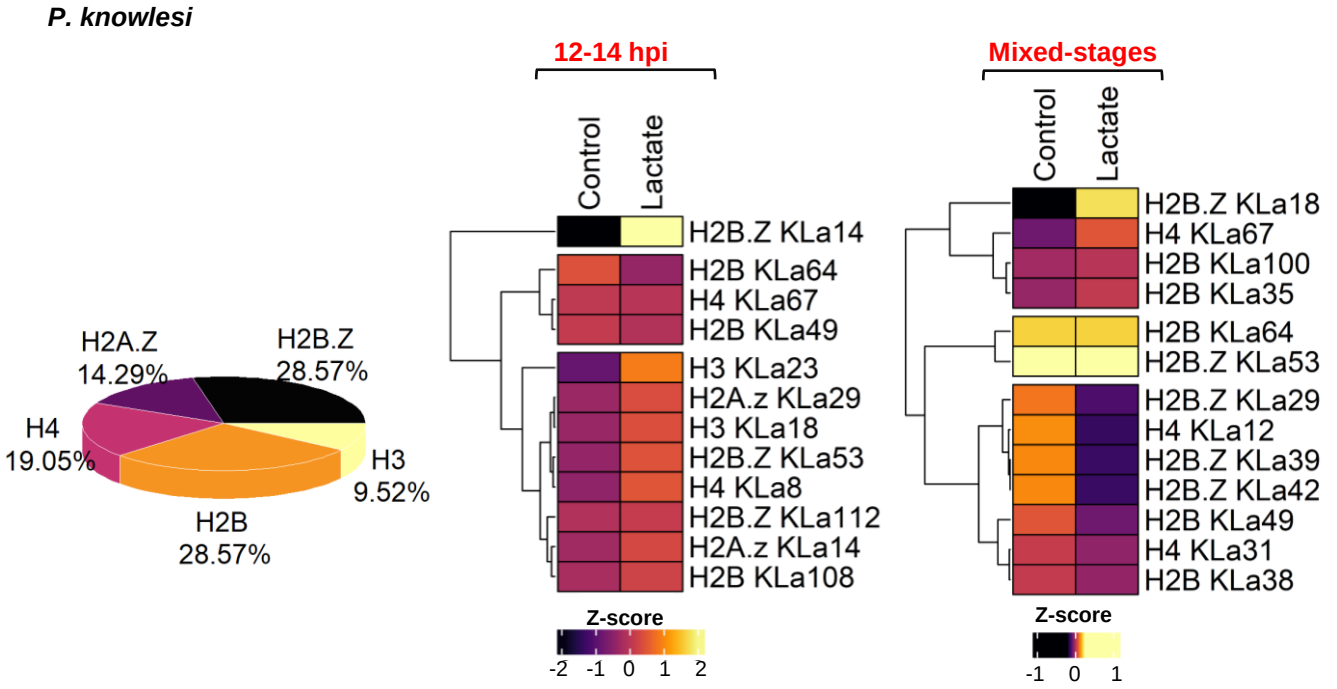
P. knowlesi
12-14 hpi
Mixed-stages
Control
Lactate
H2A.Z 14.29%
H2B.Z 28.57%
H4 19.05%
H3 9.52%
H2B 28.57%
H2B.Z KLa14
H2B KLa64
H4 KLa67
H2B KLa49
H3 KLa23
H2A.z KLa29
H3 KLa18
H2B.Z KLa53
H4 KLa8
H2B.Z KLa112
H2A.z KLa14
H2B KLa108
H2B.Z KLa18
H4 KLa67
H2B KLa100
H2B KLa35
H2B KLa64
H2B.Z KLa53
H2B.Z KLa29
H4 KLa12
H2B.Z KLa39
H2B.Z KLa42
H2B KLa49
H4 KLa31
H2B KLa38
Z-score
-2 -1 0 1 2
-1 0 1

Figure 6

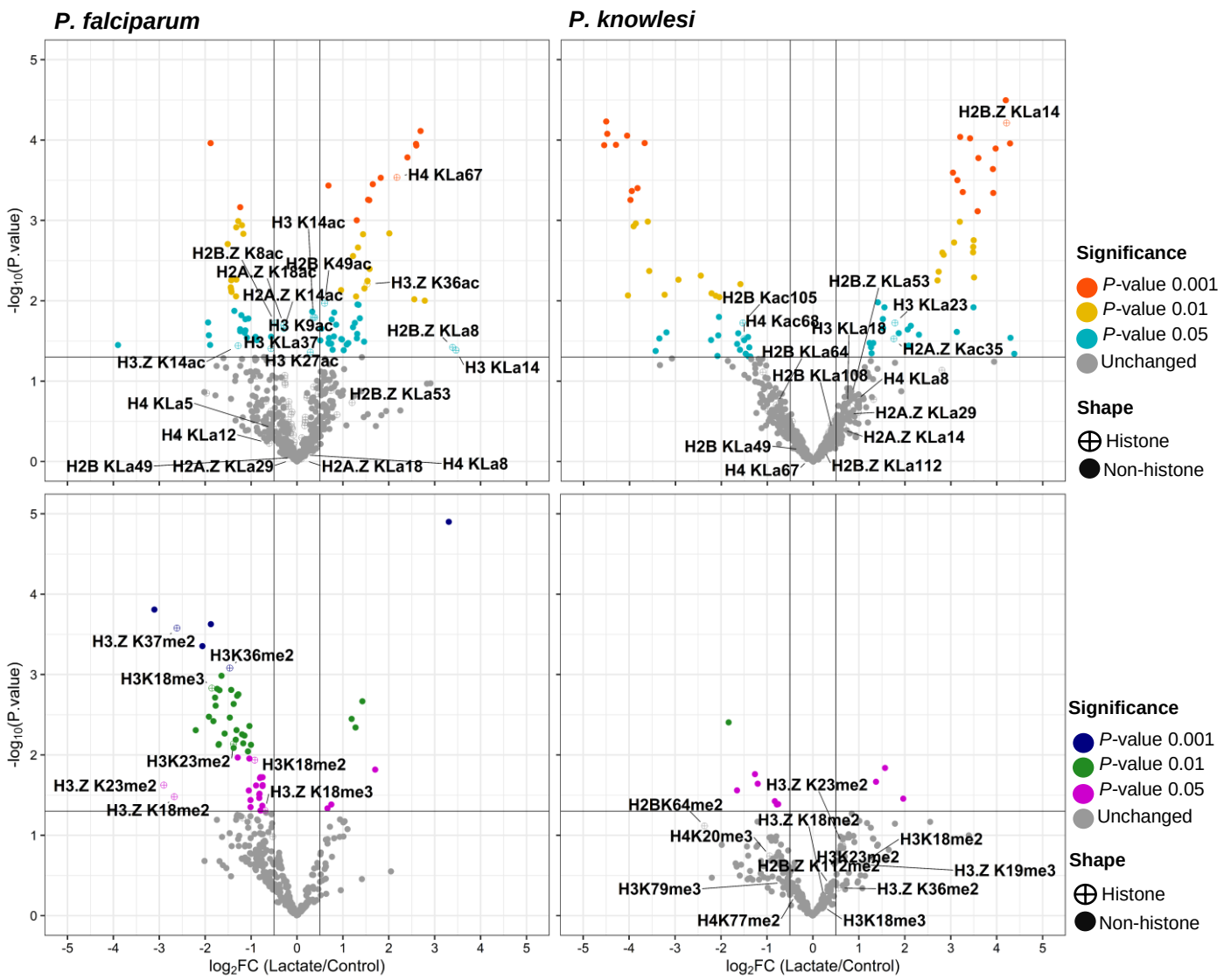
A
P. falciparum
P. knowlesi
-log10(P.value)
log2FC (Lactate/Control)
H4 KLa67
H3 K14ac
H2B.Z K8ac
H2B K49ac
H2A.Z K18ac
H3.Z K36ac
H2A.Z K14ac
H3 K9ac
H2B.Z KLa8
H3 KLa37
H3.Z K14ac
H3 K27ac
H3 KLa14
H2B.Z KLa53
H4 KLa5
H4 KLa12
H2B KLa49
H2A.Z KLa29
H2A.Z KLa18
H4 KLa8
H2B.Z KLa14
H2B.Z KLa53
H2B Kac105
H3 KLa23
H4 Kac68
H3 KLa18
H2B KLa64
H2A.Z Kac35
H2B KLa108
H4 KLa8
H2A.Z KLa29
H2A.Z KLa14
H2B KLa49
H4 KLa67
H2B.Z KLa112
Significance
P-value 0.001
P-value 0.01
P-value 0.05
Unchanged
Shape
Histone
Non-histone
H3.Z K37me2
H3K36me2
H3K18me3
H3K23me2
H3K18me2
H3.Z K23me2
H3.Z K18me3
H3.Z K18me2
H3.Z K23me2
H2BK64me2
H3.Z K18me2
H4K20me3
H3K18me2
H3K23me2
H2B.Z K112me2
H3.Z K19me3
H3K79me3
H3.Z K36me2
H4K77me2
H3K18me3
Significance
P-value 0.001
P-value 0.01
P-value 0.05
Unchanged
Shape
Histone
Non-histone

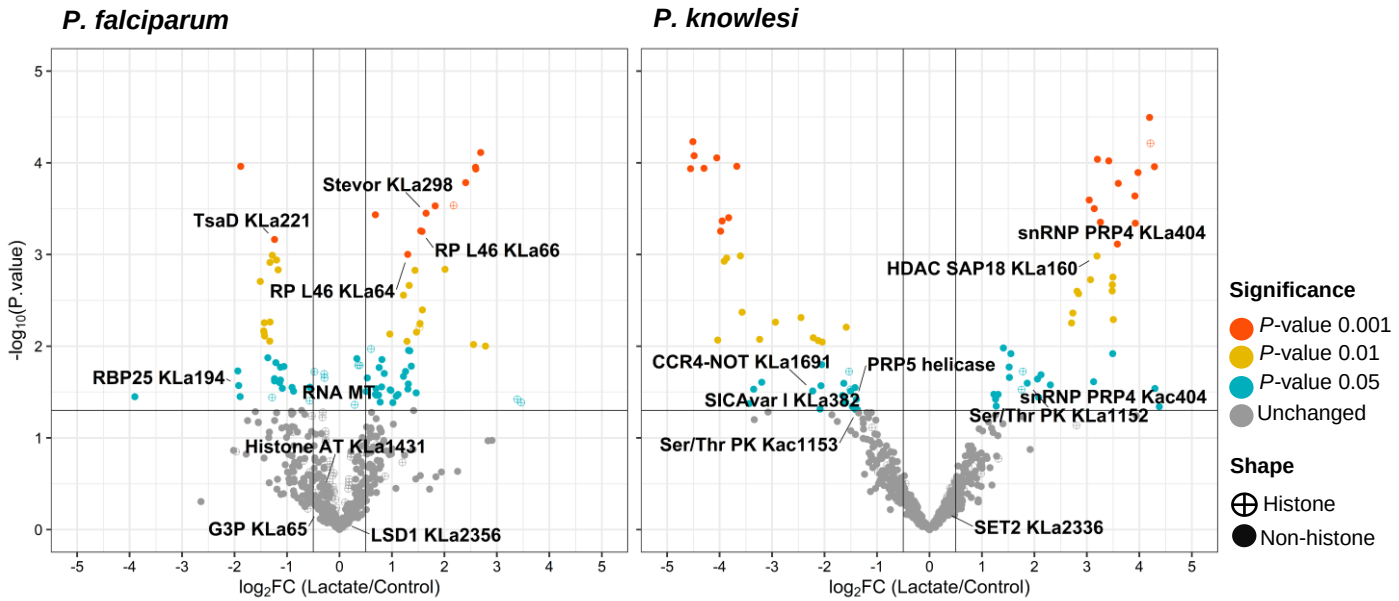
B
P. falciparum
P. knowlesi
-log10(P.value)
log2FC (Lactate/Control)
Stevor KLa298
TsaD KLa221
RP L46 KLa66
RP L46 KLa64
RBP25 KLa194
RNA MT
Histone AT KLa1431
G3P KLa65
LSD1 KLa2356
snRNP PRP4 KLa404
HDAC SAP18 KLa160
CCR4-NOT KLa1691
PRP5 helicase
SICAvar I KLa382
snRNP PRP4 Kac404
Ser/Thr PK KLa1152
Ser/Thr PK Kac1153
SET2 KLa2336
Significance
P-value 0.001
P-value 0.01
P-value 0.05
Unchanged
Shape
Histone
Non-histone

Figure 7

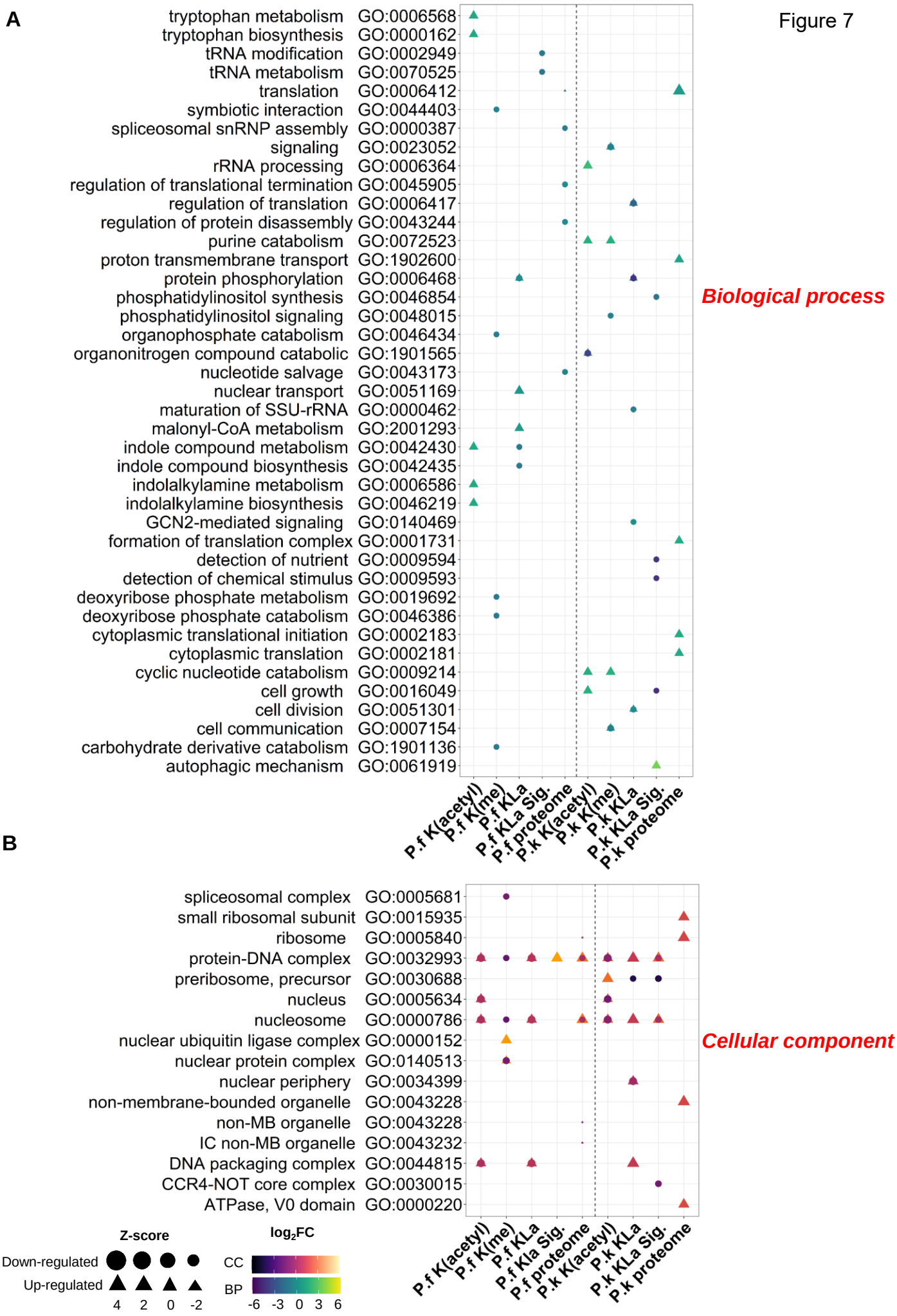
A
tryptophan metabolism GO:0006568
tryptophan biosynthesis GO:0000162
tRNA modification GO:0002949
tRNA metabolism GO:0070525
translation GO:0006412
symbiotic interaction GO:0044403
spliceosomal snRNP assembly GO:0000387
signaling GO:0023052
rRNA processing GO:0006364
regulation of translational termination GO:0045905
regulation of translation GO:0006417
regulation of protein disassembly GO:0043244
purine catabolism GO:0072523
proton transmembrane transport GO:1902600
protein phosphorylation GO:0006468
phosphatidylinositol synthesis GO:0046854
phosphatidylinositol signaling GO:0048015
organophosphate catabolism GO:0046434
organonitrogen compound catabolic GO:1901565
nucleotide salvage GO:0043173
nuclear transport GO:0051169
maturation of SSU-rRNA GO:0000462
malonyl-CoA metabolism GO:2001293
indole compound metabolism GO:0042430
indole compound biosynthesis GO:0042435
indolalkylamine metabolism GO:0006586
indolalkylamine biosynthesis GO:0046219
GCN2-mediated signaling GO:0140469
formation of translation complex GO:0001731
detection of nutrient GO:0009594
detection of chemical stimulus GO:0009593
deoxyribose phosphate metabolism GO:0019692
deoxyribose phosphate catabolism GO:0046386
cytoplasmic translational initiation GO:0002183
cytoplasmic translation GO:0002181
cyclic nucleotide catabolism GO:0009214
cell growth GO:0016049
cell division GO:0051301
cell communication GO:0007154
carbohydrate derivative catabolism GO:1901136
autophagic mechanism GO:0061919
P.f K(acetyl)
P.f K(me)
P.f KLa
P.f KLa Sig.
P.f proteome
P.k K(acetyl)
P.k K(me)
P.k KLa
P.k KLa Sig.
P.k proteome
Biological process
B
spliceosomal complex GO:0005681
small ribosomal subunit GO:0015935
ribosome GO:0005840
protein-DNA complex GO:0032993
preribosome, precursor GO:0030688
nucleus GO:0005634
nucleosome GO:0000786
nuclear ubiquitin ligase complex GO:0000152
nuclear protein complex GO:0140513
nuclear periphery GO:0034399
non-membrane-bounded organelle GO:0043228
non-MB organelle GO:0043228
IC non-MB organelle GO:0043232
DNA packaging complex GO:0044815
CCR4-NOT core complex GO:0030015
ATPase, V0 domain GO:0000220
P.f K(acetyl)
P.f K(me)
P.f KLa
P.f Kla Sig.
P.f proteome
P.k K(acetyl)
P.k KLa
P.k KLa Sig.
P.k proteome
Cellular component
Z-score
Down-regulated
Up-regulated
4 2 0 -2
log2FC
CC
BP
-6 -3 0 3 6

Figure 8

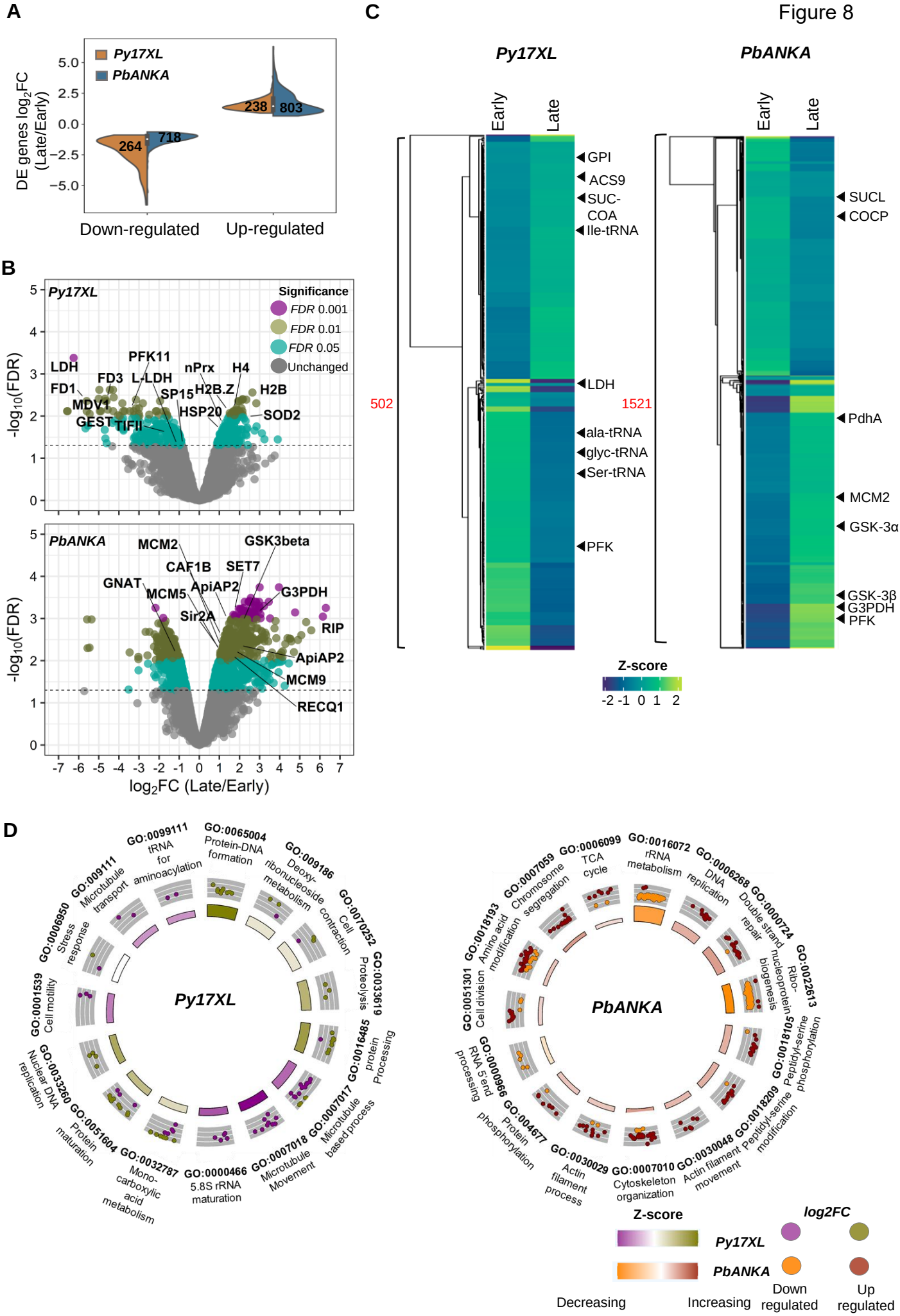
A
Py17XL
PbANKA
DE genes log2FC (Late/Early)
5.0
2.5
0.0
−2.5
−5.0
264
718
238
803
Down-regulated
Up-regulated
B
Py17XL
Significance
FDR 0.001
FDR 0.01
FDR 0.05
Unchanged
LDH
FD1
FD3
MDV1
GEST
TIFII
PFK11
L-LDH
SP15
nPrx
H2B.Z
HSP20
H4
H2B
SOD2
-log10(FDR)
PbANKA
MCM2
GSK3beta
CAF1B
SET7
GNAT
MCM5
ApiAP2
G3PDH
Sir2A
RIP
ApiAP2
MCM9
RECQ1
-7 -6 -5 -4 -3 -2 -1 0 1 2 3 4 5 6 7
log2FC (Late/Early)
C
Py17XL
PbANKA
Early
Late
GPI
ACS9
SUC-COA
Ile-tRNA
LDH
ala-tRNA
glyc-tRNA
Ser-tRNA
PFK
502
1521
SUCL
COCP
PdhA
MCM2
GSK-3α
GSK-3β
G3PDH
PFK
Z-score
-2 -1 0 1 2
D
Py17XL
GO:0099111 tRNA for aminoacylation
GO:0065004 Protein-DNA formation
GO:009186 Deoxy-ribonucleoside metabolism
GO:0070252 Cell contraction
GO:0033619 Proteolysis
GO:0016485 protein Processing
GO:0007017 Microtubule based process
GO:0007018 Microtubule Movement
GO:0000466 5.8S rRNA maturation
GO:0032787 Mono-carboxylic acid metabolism
GO:0051604 Protein maturation
GO:0033260 Nuclear DNA replication
GO:0001539 Cell motility
GO:0006950 Stress response
GO:009111 Microtubule transport
PbANKA
GO:0007059 Chromosome segregation
GO:0006099 TCA cycle
GO:0016072 rRNA metabolism
GO:0006268 DNA replication
GO:0000724 Double strand repair
GO:0022613 Ribo-nucleoprotein biogenesis
GO:0018105 Peptidyl-serine phosphorylation
GO:0018209 Peptidyl-serine modification
GO:0030048 Actin filament movement
GO:0007010 Cytoskeleton organization
GO:0030029 Actin filament process
GO:004677 Protein phosphorylation
GO:0000966 RNA 5'end processing
GO:0051301 Cell division
GO:0018193 Amino acid modification
Z-score
Decreasing
Increasing
Py17XL
PbANKA
log2FC
Down regulated
Up regulated